Multiphoton imaging of neural structure and activity in *Drosophila* through the intact cuticle

Max Jameson Aragon[1,4,#], Aaron T. Mok[2,#], Jamien Shea[1#], Mengran Wang[2,#], Haein Kim[1], Nathan Barkdull[3], Chris Xu[2] and Nilay Yapici[1,*]

[1]*Department of Neurobiology and Behavior, Cornell University, 14853, Ithaca, NY, USA*

[2]*School of Applied and Engineering Physics, Cornell University, 14853, Ithaca, NY, USA*

[3]*Department of Physics, University of Florida, 32611, Gainesville, FL, USA*

[4]*Current address: Princeton Neuroscience Institute, Princeton University, 08544, Princeton, NJ, USA*

[#]*These authors contributed equally to this work*

**Corresponding author: Nilay Yapici (ny96@cornell.edu)*

ABSTRACT

We developed a multiphoton imaging method to capture neural structure and activity in behaving flies through the intact cuticles. Our measurements show that the fly head cuticle has surprisingly high transmission at wavelengths > 900 nm, and the difficulty of through-cuticle imaging is due to the air sacs and/or fat tissue underneath the head cuticle. By compressing or removing the air sacs, we performed multiphoton imaging of the fly brain through the intact cuticle. Our anatomical and functional imaging results show that 2- and 3-photon imaging are comparable in superficial regions such as the mushroom body, but 3-photon imaging is superior in deeper regions such as the central complex and beyond. We further demonstrated 2-photon through-cuticle functional imaging of odor-evoked calcium responses from the mushroom body γ-lobes in behaving flies short-term and long-term. The through-cuticle imaging method developed here extends the time limits of *in vivo* imaging in flies and opens new ways to capture neural structure and activity from the fly brain.

INTRODUCTION

Animal nervous systems across lineages have evolved to solve many of the same problems; foraging for food and water, finding mates to reproduce, and avoiding predators to stay alive. They navigate their environment via coordinated movements and learn and remember the relative values of sensory stimuli around them to maximize their fitness and survival. At each instant in time, an animal must evaluate external sensory information and its current behavioral state to decide what to do next (Dickson, 2008; Hunt and Hayden, 2017; Lutcke et al., 2013; Tinbergen, 1969). A major technological challenge to revealing how the brain encodes behavioral states in real-time is that even the simplest neural computation involves interactions across the nervous system at various time scales, while our tools for assessing neural activity are restricted in time and space because of the currently available imaging sensors, methods, and preparations (Lerner et al., 2016). Optical methods remain the most established and fruitful path for revealing population dynamics in neural circuits at long time scales (ranging from minutes to hours) by providing high temporal and spatial resolution measurements (Ji et al., 2016; Luo et al., 2018; Svoboda and Yasuda, 2006).

The fly, *Drosophila melanogaster*, offers an ideal experimental system to investigate neural correlates of behavioral states and decisions because of its compact nervous system and diverse state-dependent behaviors that it executes in response to sensory stimuli (Barron et al., 2015; Dickson, 2008). To understand how molecularly defined neural circuits evaluate sensory information in different behavioral states, it is critical to capture the activity of populations of neurons over long time scales as flies are changing their physiological needs (Luo et al., 2018; Simpson and Looger, 2018). These functional imaging experiments require imaging preparations, which should allow chronic neural activity imaging for at least 12 hours. Current methods used in fly optical physiology require the fly head cuticle, trachea, and fat body to be removed by microsurgery to provide optical access to the nervous system (Grover et al., 2016; Minocci et al., 2013; Seelig et al., 2010; Sinha et al., 2013; Wang et al., 2003). These preparations are limited in imaging duration because after some time, the brain tissue starts to degenerate due to damaged circulation resulting from the cuticle removal surgery. For example, with current imaging preparations, fly olfactory neurons show reliable Ca^{2+} responses for four to five hours after surgery (Wang et al., 2003). An imaging method

in which the head cuticle is intact, thereby eliminating the need for traumatic head surgery before functional imaging, is essential for advancing fly neuroscience research in the direction of chronic recordings of neural activity during ongoing behaviors. This includes being able to image the same fly brain across multiple days. In mice, multi-day imaging experiments are achieved by implanting a cranial window following removal of part of the skull (Hefendehl et al., 2012; Trachtenberg et al., 2002). Similar imaging preparations have been developed for flies (Grover et al., 2016; Huang et al., 2018; Sinha et al., 2013). However, because imaging window implantation requires a tedious surgery with low success rates and complications that occur afterwards, these methods are not commonly used. A recent development in *in vivo* multiphoton imaging is the use of long wavelength lasers in 3-photon (3P) microscopy which improves the signal-to-background ratio by several orders of magnitude compared to current 2-photon (2P) imaging methods (Horton et al., 2013; Wang et al., 2018a; Wang et al., 2018b). While 3P microscopy with 1700 nm excitation of red fluorophores and adaptive optics has shown promising results in imaging the fly brain through the cuticle (Tao et al., 2017), it is not clear if the technique is widely applicable to common blue and green fluorophores with much shorter excitation wavelengths (e.g. 1320nm).

Here, we developed a method for imaging fly neural structure and activity through the intact head cuticle using both 2P and 3P microscopy. We first measured the ballistic and total optical transmission through the dorsal fly head cuticle and surprisingly found that the head cuticle has high transmission at the wavelengths that are used to excite green fluorophores in 2P and 3P microscopy (~920 nm and ~1320 nm, respectively). We showed that the tissue that interferes with the laser light and limits imaging through the cuticle into the brain is not the head cuticle but the air sacs and the tissue underneath the cuticle. Next, we developed fly preparations by either compressing the air sacs or removing them from the imaging window allowing through-cuticle imaging of the fly brain. Using these imaging preparations, we performed deep, high spatial resolution imaging of the fly brain and determined the attenuation length for imaging through the cuticle with 2P (920 nm) and 3P (1320 nm) excitation and compared our results to cuticle-removed preparations. Our measurements showed that 2P and 3P excitation performed similarly in shallow regions (i.e., in the mushroom body) of the fly brain, but 3P excitation at 1320 nm is superior for

imaging neural activity and anatomical features in deeper brain structures (i.e., in the central complex). Furthermore, using 2P and 3P excitation, we recorded food odor evoked neural responses from Kenyon cells comprising the mushroom body γ-lobes using a genetically encoded Ca^{2+} indicator, GCaMP6s (Chen et al., 2013). In our simultaneous 2P and 3P functional imaging experiments, we found no differences between 2P and 3P excitation, while recording odor evoked responses from the mushroom body γ-lobes through the cuticle. To demonstrate that our cuticle-intact imaging method can be used for recording neural activity in behaving flies, we used 2P excitation and captured odor evoked neural responses from mushroom body γ-lobes in flies walking on an air suspended spherical treadmill. Finally, we demonstrated long-term functional imaging by reliably capturing odor evoked neural responses from γ-lobes with 2P excitation for 12 consecutive hours. The cuticle-intact imaging method developed here allows multiphoton imaging of the fly brain through the head cuticle opening new ways to capture neural structure and activity from the fly brain at long time scales and potentially through the entire lifespan of flies.

RESULTS

Fly head cuticle transmits long wavelength light with high efficiency

To develop a cuticle-intact imaging method using multiphoton microscopy, we first measured light transmission at different wavelengths through the fly head cuticle. Previous experiments showed that, within the wavelength range of 350 nm to 1000 nm, the relative transmission of the dorsal head cuticle of *Drosophila melanogaster* improves with increasing wavelengths (Lin et al., 2015). However, the absolute transmission, which is critical for assessing the practicality of through-cuticle imaging, was not reported. In our experiments, we quantified both the total and ballistic transmission of infrared (IR) laser lights through the cuticle using the setup from our previous work (Mok et al., 2022). Dissected head cuticle samples were mounted between two glass coverslips and placed in the beam path between the laser source and the photodetector (Figure 1A). The total and ballistic transmission through the cuticle samples were measured using a custom-built system (Figure 1B). For ballistic transmission, light from a single-mode fiber was magnified and focused on the cuticle with a ~25µm spot size. Figure 1C illustrates the light path of ballistic transmission experiments. The

sample stage was translated to obtain measurements at different locations on the head cuticle. Ballistic transmission through the cuticle was measured at seven different wavelengths (852 nm, 911 nm, 980 nm, 1056 nm, 1300 nm, 1552 nm, 1624 nm) that match the excitation wavelengths for typical 2P and 3P imaging. We found that for all the IR wavelengths tested, the ballistic transmission through the cuticle was high, reaching >90% at 1300 nm (Figure 1D, Figure_1_source_data_1). Since fluorescence signal within the focal volume in 2P- and 3P-microscopy is mostly generated by the ballistic photons (Dong et al., 2003; Horton et al., 2013), our results showed that ballistic photon attenuation by the fly cuticle does not limit multiphoton imaging through the intact cuticle.

To assess the absorption properties, we measured the total transmission through the head cuticle. For these measurements, laser light from a single mode fiber was magnified and focused on the cuticle sample with a ~50μm spot size (Mok et al., 2022). An integrating sphere was placed immediately after the cuticle to measure the total transmission. Figure 1F illustrates the light path of total transmission experiments. Total transmission through the cuticle was measured at nine different wavelengths (514 nm, 630 nm, 852 nm, 911 nm, 980 nm, 1056 nm, 1300 nm, 1552 nm, 1624 nm). The shorter wavelengths of 514 nm and 630 nm were chosen to match the typical fluorescence emission wavelengths of green and red fluorophores. Similar to the ballistic transmission experiments, we found that the total transmission generally increases with wavelength (Figure 1G, Figure_1_source_data_1), and the total transmission for both the green and red wavelengths was sufficiently high (>60%) for practical epi-fluorescence imaging using 2P or 3P excitation. We also scanned the cuticle with a motorized stage in the setup at selected wavelengths (Figure 1E and H), and these spatially resolved transmission maps confirmed that there are only a few localized regions at the periphery of the cuticle with low transmission. Our results demonstrated that absorption and scattering of long wavelength light by the *Drosophila* head cuticle is small, and cuticle-intact *in vivo* imaging of green (e.g., GFP and GCaMP) and red fluorophores (e.g., RFP, RCaMP) through the intact cuticle is possible in adult flies using 2P or 3P excitation.

Through-cuticle multiphoton imaging of the fly brain

Based on our cuticle transmission results, we developed a cuticle-intact imaging method where we either used head compression to minimize the volume of the air sacs (Figure 2A, Video 1) or removed them completely from the head capsule (Figure 2-figure supplement 1B-D). Using our new fly preparations, we imaged the fly brain through the cuticle with no head compression, semi-compression, or full-compression (Figure 2B-D). We expressed membrane-targeted GFP selectively in mushroom body Kenyon cells and scanned the fly brain through the cuticle using 2P and 3P excitation at 920 nm and 1320 nm, respectively (Figure 2E-G). Kenyon cells are the primary intrinsic neurons in the insect mushroom body. Diverse subtypes of Kenyon cells (n=~2200) extend their axons along the pedunculus and in the dorsal and medial lobes (Crittenden et al., 1998; Ito et al., 1998; Strausfeld et al., 1998). These neurons receive and integrate information from heterogeneous sets of projection neurons which carry olfactory, gustatory, and visual sensory information (Owald and Waddell, 2015; Yagi et al., 2016). Kenyon cell dendrites arborize in the calyx, while their axons fasciculate into anatomically distinct structures called lobes, with the dorsal lobes forming α and α′ branches, and the medial lobes containing β, β′, and γ branches (Crittenden et al., 1998; Ito et al., 1998; Zheng et al., 2018). We used transgenic flies that specifically expressed membrane targeted GFP in Kenyon cells forming α, β and γ lobes (Krashes et al., 2007). In non-compressed flies, the mushroom body lobes were barely visible in both 2P and 3P imaged flies. Compressing the head against the cover-glass with forceps during the curing process drastically improved image quality (Figure 2E-G), mushroom body lobes were clearly visible in semi-compressed and compressed preparations in both 2P and 3P imaged flies. Based on our observations of the leg movements, flies behaved similarly in semi-compressed and non-compressed preparations but not in full compression. We also tested the male courtship behavior of flies whose heads were previously semi-compressed. Our results showed that semi-head compression does not affect male courtship behavior grossly; head-compressed males are able to copulate with females at similar rates as control males (Figure 2- figure supplement 1A). Based on our imaging and behavior results, we decided to use the semi-compressed preparation in our experiments.

Why does head compression improve image quality during 2P and 3P imaging? We hypothesized, head compression might reduce the volume of air sacs and the surrounding tissue between the cuticle and the brain, allowing better transmission of long wavelength laser light through these structures. To test our hypothesis, we surgically removed air sacs from one side of the fly head and imaged the brain using 2P and 3P excitation without any head compression. As predicted, we were able to image the mushroom body lobes on the side where air sacs were removed but not on the side where intact air sacs were present (Figure 2- figure supplement 1B-D, Video 2). Our results demonstrated that the tissue that interferes with 2P and 3P laser light is not the cuticle itself but the air sacs and other tissues that are between the head cuticle and the brain.

Comparison of 2P and 3P excitation for deep brain imaging through the fly head cuticle

Our experiments showed that through–cuticle imaging is possible with both 2P and 3P excitation. In general, 3P excitation requires higher pulse energy at the focal plane compared to 2P excitation because of the higher-order nonlinearity. On the other hand, longer wavelength (1320 nm) used for 3P excitation can experience less attenuation while travelling in the brain tissue leading to increase tissue penetrance and imaging depth (Wang et al., 2018a). To compare the performance of 2P and 3P excitation for through-cuticle imaging, we imaged the entire brain in a fly expressing membrane-targeted GFP pan neuronally. Figure 3A shows the images from the same fly brain at different depths obtained with 2P (920 nm) and 3P (1320 nm) excitation. At the superficial brain areas such as the mushroom bodies, 2P and 3P excitation performed similarly. As we imaged deeper in the brain, 3P excitation generated images with higher contrast compared to 2P excitation and was capable of imaging brain regions below the esophagus. We further quantified the effective attenuation length (EAL) for 2P and 3P excitation, and we found EAL_{920nm}= 41.7 µm, EAL_{1320nm}= 59.4 µm within depth 1-100µm, and EAL_{1320nm}= 91.7 µm within depth 100-180µm (Figure 3B, Figure_3_source_data_1). The third harmonic generation (THG) signal from the head cuticle and the trachea was also measured as a function of depth. THG signal can be used to measure the EAL (EAL_{THG}) (Yildirim et al., 2019). The EAL_{THG} within the cuticle was much larger than the EAL_{THG} inside the brain, once again demonstrating the high ballistic transmission of the 1320 nm laser light

through the head cuticle (Figure 3C, Figure_3_source_data_1). The full width at half maximum (FWHM) of the lateral brightness distribution at 200μm below the surface of the cuticle was ~1.4μm for tracheal branches captured by the THG signal (Figure 3D). Similarity in the attenuation lengths of THG and 3P fluorescence signal indicates that the labelling of membrane targeted GFP is uniform across the brain, validating the use of the fluorescence signal when quantifying the EALs.

Cuticle-removed preparations are widely used in the fly neuroscience imaging studies (Seelig et al., 2010; Simpson and Looger, 2018; Wang et al., 2003). To directly compare the spatial resolution of cuticle-intact and cuticle-removed imaging preparations, we imaged the entire brain in flies expressing membrane-targeted GFP pan neuronally. We found that in the superficial layers of the fly brain (i.e., ~50 μm), through cuticle 2P and 3P imaging generated images with similar signal-to-background ratio (SBR) to cuticle-removed preparation (Figure 3 - figure supplement 1A and B). We were able to distinguish the Mushroom body and the central complex neuropils clearly in both imaging preparations. 3P generated images with better SBR compared to 2P in both cuticle-intact and cuticle-removed preparations. We measured the effective attenuation length (EAL) for both cuticle-removed and cuticle-intact 2P/3P imaging and found that removing the cuticle and underlying tissues increased the EAL by ~1.5X (Figure 3 - figure supplement 1C and D, Figure_3-figure_S1_source_data_1). As the imaging depth increases, the image contrast decreases. The degradation of the image contrast in both 2P and 3P images is manifested by the change of the slope (Akbari et al., 2022; LaViolette and Xu, 2021) in the semi-log plot of fluorescence signal versus depth (Figure 3 - figure supplement 1C and D). Within ~100 μm depth, 2P imaging provided reasonable contrast when imaging through intact cuticle. While imaging is still possible with 3P at the sub-esophageal zone (>150μm), it shows an increase in background that degrades image contrast when imaging beyond the esophagus (~150μm). When cuticle was removed, 2P imaging depth increased to ~ 180μm, and 3P imaging depth increased to ~300μm, reaching to the bottom of the fly brain. We further quantified and compared the laser power required to obtain the same fluorescence signal of 0.1 photon per laser pulse. For cuticle-removed fly, 3P requires 1.4nJ and 2P

requires 0.2nJ on the brain surface to image the mushroom body. For cuticle-intact fly, 3P requires 3.0nJ and 2P requires 0.5nJ on the cuticle surface to image the mushroom body.

2P/3P imaging of mushroom body and central complex neurons through the fly head cuticle

To further test the performance of through-cuticle imaging with 2P and 3P excitation, we imaged the central complex ellipsoid body ring neurons. The insect central complex is a brain neuropil which processes sensory information and guides a diverse set of behavioral responses (Pfeiffer and Homberg, 2014; Seelig and Jayaraman, 2015; Wolff et al., 2015). It is composed of anatomically distinct compartments: the protocerebral bridge, ellipsoid body, fan-shaped body, and the noduli (Wolff et al., 2015). The ellipsoid body consists of a group of neurons, the ring neurons, that extend their axons to the midline forming a ring-like structure (Pfeiffer and Homberg, 2014; Wolff et al., 2015; Xie et al., 2017). Using an ellipsoid body-specific promoter, we expressed a membrane-targeted GFP in the ring neurons and imaged them with 2P and 3P. Compared to 3P (Figure 3E, Video 3), the resolution and contrast of images taken by 2P is reduced when imaging through the cuticle at this depth (Figure 3-figure supplement 2E). Using ring neuron arbors and tracheal branches, we estimated the lateral resolution of the 3P images. The FWHM of the lateral brightness distribution measured by a ring neuron's neurite cross section was ~1.2μm for the fluorescent signal (Figure 3F) and ~0.8μm for tracheal branches captured by the THG signal (Figure 3G).

Next, we investigated whether cellular and subcellular resolution is achievable using the cuticle-intact imaging preparation and compared our results to cuticle-removed 2P and 3P imaging. For these experiments, we imaged the Kenyon cells and the ellipsoid body ring neurons expressing a membrane targeted GFP. Our data showed that Kenyon cell bodies are visible with cuticle-intact 2P and 3P imaging (Figure 3-figure supplement 3A and E), while deeper ellipsoid body ring neurons are only clearly distinguishable with 3P imaging (Figure 3-figure supplement 2A and E). Our measurements showed that the cuticle-removed imaging preparation generated images with ~1.5X better axial resolution compared to cuticle-intact imaging preparations for both 2P and 3P imaging (Figure 3-figure supplement 2 and 3, Figure_3-figure_S2_source_data_1, Figure_3-figure_S3_source_data_1). 3P imaging shows the same axial resolution in the mushroom body

(~50 µm) and central complex (~100 µm) while 2P imaging shows a deterioration of axial resolution for deep imaging in the central complex (Figure 3-figure supplement 2 and 3). We also investigated imaging stability during through cuticle imaging by tracking ellipsoid body cell bodies in flies walking on a ball (Video 4). We did not detect major changes in the fluorescence intensity during walking. The average motion measured was 1.3 µm, which is much smaller than the size of a fly neuron (~5 µm) (Figure 3-figure supplement 4. Figure_3-figure_S4_source_data_1). Based on our results, we concluded that motion is not an issue during through-cuticle imaging at depths we have investigated. Together our results demonstrate that although both 2P and 3P excitation can be used for cuticle through imaging at the superficial layers of the fly brain such as the mushroom body, 3P outperforms 2P in deeper brain regions such as the central complex especially when cellular and subcellular resolution is necessary. This conclusion is consistent with the imaging studies conducted in the mouse brain (Mok et al., 2019; Wang et al., 2018a; Wang et al., 2020).

2P and 3P through cuticle imaging does not induce heating damage to the fly brain tissue

The recommended power level for 2P imaging of fly neural activity with cuticle-removed preparations is ~15mW (Seelig et al., 2010). However, it is not known what the safe power levels for 2P and 3P imaging are, when imaging through the cuticle. It has been shown 3P excitation can induce heating in the mouse brain at high laser powers (Wang et al., 2018a; Wang et al., 2018b; Wang et al., 2020). Therefore, we measured how heat generated by 2P and 3P excitation impacts the fly brain using HSP70 protein as a marker for cellular stress response (Lindquist, 1980; Podgorski and Ranganathan, 2016). We first tested whether HSP70 protein levels reflect heat induced stress in the fly brain. Flies that were kept at room temperature had low levels of the HSP70 protein (Figure 4-figure supplement 1A). In contrast, placing flies in a 30^{o}C incubator for 10 minutes caused a significant increase in HSP70 protein levels across the fly brain (Figure 4-figure supplement 1B). Next, we tested whether 2P and 3P excitation causes an elevation in HSP70 protein levels when imaging through the cuticle. Head-fixed flies in a semi-compressed imaging preparation were imaged either with 3P or 2P excitation. Our results showed that there was no measurable heat-stress response detected by the HSP70 protein levels when flies were exposed to

2P (920nm) and 3P (1320nm) excitation at 15mW for 24 minutes (four 6-minute intervals, see methods for details) (Figure 4-figure supplement 1C-E). However, increasing laser power to 25mW for 3P caused a significant increase in HSP70 protein levels in the fly brain (Figure 4-figure supplement 2F). These results suggest that 2P and 3P cuticle-intact imaging is safe at power levels below 15mW, similar to power levels used for 2P cuticle-removed imaging.

Whole brain 2P and 3P imaging in response to electrical stimulation

Encouraged by our structural imaging results, we next tested the applicability of 2P and 3P microscopy to capture neural activity in the entire fly brain through the intact head cuticle. In these experiments, we used a mild electric shock (1s, ~5V), and recorded neural activity in flies expressing GCaMP6s pan-neuronally. We imaged the entire fly brain using the cuticle-intact and cuticle-removed imaging preparations with 2P and 3P. As expected, electrical stimulation generated a neural response in all the ROIs recorded across different depths of the fly brain. 3P cuticle-removed preparation allowed us to image down to ~250μm deep (Figure 4B), while the depth limit for 3P cuticle-intact imaging was ~120μm (Figure 4A). Additionally, we found that dF/F_o for 3P cuticle-removed imaging preparation was between 0.2 to 0.7 and for cuticle-intact imaging preparation it was between 0.2 to 0.5 (Figure 4A and B). We repeated the depth and dF/F_o analysis for 2P cuticle-intact and cuticle removed imaging. The depth limit for 2P functional imaging through the cuticle was ~65 μm, while cuticle-removed imaging allowed optical access to ~120μm (Figure 4C and D, Figure_4_source_data_1). The dF/F_o for 2P cuticle-removed imaging preparation ranged between 0.2 to 0.4, while in the cuticle-intact preparation it was between 0.2 to 0.3. These results suggested that the presence of the cuticle and the underlying tissue decreases 2P and 3P functional imaging depth in the brain by ~ 2x and reduces dF/F_o. Similar to structural imaging, 3P outperforms 2P at deeper regions of the fly brain when recording neural activity in both cuticle-intact and cuticle-removed imaging preparations.

Simultaneous 2P and 3P imaging of odor responses from Mushroom body gamma-lobes

We next recorded neural responses in the fly brain through the intact cuticle using a more natural stimulus, food odor. In these experiments, a custom odor delivery system was used where flies were head-fixed and standing on a polymer ball under the microscope (Figure 5A and B). We expressed GCaMP6s in the Mushroom body Kenyon cells and stimulated the fly antenna with the food odor apple cider vinegar (Figure 5C). Using a multiphoton microscope, odor evoked Ca^{2+} responses of mushroom body γ-lobes were simultaneously captured with 2P (920 nm) and 3P (1320 nm) excitation using the temporal multiplexing technique (Ouzounov et al., 2017). A brief 3s odor stimulus triggered a robust fluorescence increase in the mushroom body γ-lobes (Figure 5F). Based on dopaminergic innervation, γ-lobes can be subdivided into five anatomical compartments (Cohn et al., 2015) (Figure 5D and E). To investigate whether food odor is represented by different spatio-temporal patterns in the γ-lobe compartments, we calculated the normalized fluorescence signal for each compartment. No significant differences were observed in neural activity in responses to food odor stimulation across different compartments of the γ-lobes or between 2P and 3P excitation of GCaMP6s (Figure 5G-I, Figure 5-figure-supplement 1, Figure_5_source_data_1). We also recorded neural activity from Kenyon cell bodies in response to olfactory stimulation using 3P excitation (Figure 5-figure supplement 2). Our data demonstrated that both 2P and 3P excitation can be used to image odor responses from mushroom body γ-lobes using through-cuticle imaging but for cell body imaging 3P excitation is preferred.

2P through-cuticle imaging captures odor evoked responses in behaving flies

To investigate how head compression impacts fly behavior and neural activity, we investigated how flies that are head-compressed but allowed to walk on a spherical treadmill respond to an odor stimulation. Using our custom behavior/imaging setup (Figure 6A), we stimulated the fly antennae with food odor (apple cider vinegar), while recording neural activity from the mushroom body γ-lobes using 2P excitation (920 nm) through the head cuticle. In these experiments, we also captured fly's behavioral responses using a camera that is synchronized with the 2P microscope. A head-fixed fly was continuously exposed to a low-speed air flow before and after the 3s odor stimulus with the

same air flow speed, and the behavioral responses of flies were captured by tracking the spherical treadmill motion using the FicTrac software during each trial (Video 5). Because internal states impact behavioral responses to food odors (Lin et al., 2019; Sayin et al., 2019), we used flies that are 24-hour food deprived. Previous studies have demonstrated that during food odor exposure, hungry flies increase their walking speed, orient, and walk towards the odor stimulus. After odor stimulation however, flies increase their turning rate which resembles local search behavior. The odor offset responses persist for multiple seconds after the odor exposure (Alvarez-Salvado et al., 2018; Sayin et al., 2019). In our experiments with semi head-compressed flies, flies increase their turning rate upon brief stimulation with food odor apple cider vinegar (Figure 6B, Figure_6_source_data_1). During these experiments, we were able to capture odor evoked neural responses from all mushroom body γ-lobe compartments reliably (Figure 6C, Figure_6_source_data_1).

We further analyzed the odor evoked changes in fly walking behavior and showed that after the brief exposure to food odor stimulus, flies increased their forward walking speed and turning rate (Figure 6E-G, Figure_6_source_data_2). These responses lasted for multiple seconds (Figure 6H-K). Moreover, statistical analysis showed that there is a significant difference between the average forward and rotational speed values before and after the food odor exposure (Figure 6I and K, Figure_6_source_data_2). Our results are in agreement with previous studies that quantified odor induced changes in walking behavior in head-fixed flies (Sayin et al., 2019). Altogether, these results indicate that head-compressed flies in our spherical treadmill setup can walk and exhibit behavioral and neural responses to odor stimulation.

2P through-cuticle imaging captures chronic odor evoked responses

Studying how neural circuits change activity during learning or in alternating behavioral states requires chronic imaging methods that permit recording neural activity over long time scales. Leveraging our preparation, we pushed the limits of functional imaging of the fly brain in response to food odor stimulation at longer time scales (12 hours). Using a custom odor delivery system, we stimulated the fly antenna with food odor (apple cider vinegar) every four hours while imaging

through the head cuticle using 2P excitation (920 nm) (Figure 7A, Video 6). We calculated the normalized peak fluorescent signal per fly in each γ-lobe compartment and time point as a metric representing the food odor response strength during chronic imaging (Figure 7B-E, Figure_7_source_data_1-4). Our analysis showed that the odor-evoked neural responses did not change with food and water deprivation in any of the γ-lobe compartments imaged (Figure 7F, Figure_7_source_data_1_5). During these long-term imaging experiments, we captured the fly's behavior in parallel with the odor stimulation to assure that the fly stayed alive during long-term imaging (Video 6). These results suggest that the cuticle-intact imaging method developed here allows recording of neural activity within an individual fly over long-time scales (12hours), which was previously not possible with commonly used cuticle-removed imaging preparations.

DISCUSSION

Imaging through the fly cuticle was considered to be not feasible at the wavelengths typically used for 2P (~ 920 nm) and 3P (~ 1300 nm) imaging because of concerns about cuticle absorption (Lin et al., 2015; Tao et al., 2017). By quantitatively measuring the optical properties of the fly cuticle at wavelengths that correspond to 2P and 3P imaging, we discovered that fly cuticle transmits long wavelength light with surprisingly high efficiency (Figure 1). We found that it is not the absorption by the cuticle but rather the opacity of the air sacs and the tissues located between the head cuticle and the brain that limit the penetration depth of multiphoton imaging (Video 2). By compressing the fly head using a glass coverslip, we reduced the volume of the air sacs between the cuticle and the brain, which increases the transmission of laser light and therefore allows high resolution imaging of the fly brain through the intact cuticle (Figure 2). Careful assessments showed that such a head compression does not cause measurable differences in fly courtship Figure2-figure supplement 1A), or olfactory behaviors (Figure 6). Our results clearly demonstrate that long excitation wavelength (e.g., ~ 1700 nm) is not necessary for imaging the fly brain through the cuticle and our fly preparations enable cuticle-intact 2P and 3P imaging of common fluorophores (e.g., GFP and GCaMPs) at 920 nm and 1320 nm, respectively (Figure 2-7). While we did not see noticeable differences in the recorded activity traces when performing simultaneous 2P and 3P functional

imaging of the mushroom body, 3P imaging has a better SBR than 2P imaging in the deeper regions of the fly brain such as the central complex.

Investigating how physiological states, sleep, and learning change the function of neural circuits requires tracking the activity of molecularly defined sets of neurons over long time scales. These experiments require long term imaging methods to record neural activity *in vivo*. The through-cuticle imaging method developed here significantly extends the time frame of current *in vivo* imaging preparations used for anatomical and functional studies in fly neuroscience. Our imaging method will allow researchers to capture the activity of neural populations during changing behavioral states; facilitate decoding of neural plasticity during memory formation; and might permit observation of changes in brain structures during development and aging. Our first demonstration of long-term functional imaging of the fly brain captures food odor responses from mushroom body γ-lobes for up to 12 hours continuously. Our results suggest that odor evoked Ca^{2+} responses did not change during the repeated odor stimulation. Even longer imaging time is possible by feeding flies under the microscope. We performed 2P imaging for demonstrating the possibility of long-term recording of neural activity because conventional 2P microscopy has adequate penetration depth for imaging the behavioral responses within the mushroom body, and 2P microscopy is widely used by the fly neuroscience community. On the other hand, our deep functional imaging data (Figure 4) showed that combination of our cuticle-intact fly preparation and 3P imaging may provide the exciting possibility of long-term imaging in deeper regions of the fly brain such as the central complex. We note that the success rate of chronic imaging experiments was ~50% because of the drift in the axial position of the brain when imaging for long periods of time. Further optimizations might improve the success rate of chronic imaging. Our focus here was to develop cuticle-intact in vivo structural and functional imaging methods that can extend imaging quality and length for the fly brain. We anticipate that there will be a wide variety of uses for this technology in *Drosophila* neuroscience research.

ACKNOWLEDGEMENTS

We thank Joe Fetcho, Andy Bass, David Owald, and members of the Yapici Lab for comments on the manuscript. We acknowledge Bloomington Drosophila Stock Centre (NIH P40OD018537) and the Developmental Studies Hybridoma Bank (NICHD of the NIH, University of Iowa) for reagents. We thank Li Yan McCurdy (Yale University) and Matt Einhorn (Cornell University) for help with the design and construction of the custom built olfactometer, and Nancy M. Bonini (University of Pennsylvania) for her advice on the HSP70 antibody. Research in N.Y.'s laboratory is supported by a Cornell University Nancy and Peter Meinig Family Investigator Program, a Pew Scholar Award, the Alfred P. Sloan Foundation Award, AFAR Research Grant for Junior Faculty, NSF NeuroNex Program Grant (DBI-1707312), NIH R35 ESI-MIRA Grant (R35GM133698-01) and a Cornell Neurotech Mong fellowship.

FIGURE LEGENDS

Figure 1. Ballistic and total optical transmission of the fly head cuticle. (**A)** Schematic of the cuticle preparation. **(B)** Schematic of the cuticle optical transmission measurement setup. (**C)** Schematic of the ballistic optical transmission through the cuticle. (**D**) Results of the ballistic optical transmission experiments at various wavelengths (n = 56 measurements at each wavelength, 5 different samples). **(E)** Spatially resolved maps at 911 nm and 1300 nm with the percent ballistic transmission color coded. Lighter colors indicate higher transmission and darker colors indicate lower transmission. (**F)** Schematic of the total optical transmission through the cuticle. (**G)** Results of the total optical transmission experiments at various wavelengths (n = 20 measurements at each wavelength, 4 different samples). (**H**) Spatially resolved maps at 514 nm and 630 nm with the percent total transmission color coded. Lighter colors indicate higher transmission and darker colors indicate lower transmission. One-way ANOVA with post-hoc Tukey's test. Data points labeled with different letters in D and G are significantly different from each other (Scale bars =100µm).

Figure 2. **Through-cuticle imaging of the fly brain with 2P and 3P excitation.**

(A), Schematic of the multiphoton microscope setup. Fly head is fixed to a cover slip and placed under the objective (HWP: half-wave plate, PBS: polarization beam splitter, PMT: photomultiplier tube). The imaging window on the fly head is shown in the picture (lower left). Scale bar = 200µm **(B-D)**, The head-uncompressed and head-compressed imaging preparations. The first column shows the side image of the fly that is head-fixed to the cover glass (scale bar =1mm). The second and third columns show the fly head visualized under a brightfield (top view) and fluorescent dissecting microscopes (widefield-fluo), respectively. Arrows and the rectangle area in widefield-fluo column indicate the imaging window (scale bar=200µm). (**E-G),** Cross section imaging of the mushroom body (MB) Kenyon cells expressing CD8-GFP through the head cuticle at 920 nm (2P) and 1320 nm (3P) excitation. The Z projections of 2P (cyan, left) and 3P (green, right) imaging stacks. For each imaging preparation, the same fly head is imaged with 3P and 2P excitation (scale bar=20µm).

Figure 3. 2P and 3P structural imaging of the fly brain.

(A) Cross section images of the fly brain through the cuticle with 3P (top) and 2P (bottom) excitation at different depth. The THG images are included at the bottom. 3P excitation power is < 11mW and the repetition rate is 333 kHz. 2P excitation power is < 15mW and the repetition rate is 80 MHz, scale bars = 50µm. (**B**) GFP signal as a function of depth for 920 nm 2P excitation and 1320 nm 3P excitation. (**C**) Comparison of the GFP signal and THG signal as a function of depth at 1320 nm. (**D)** Lateral resolution measurement in the THG image captured at 200µm depth**.** Lateral intensity profile measured along the white line (indicated by the orange arrow) is fitted by a Gaussian profile for the lateral resolution estimation (scale bar=50µm). **(E)** Cross section images of the central complex (CC) ring neurons through the cuticle with 1320 nm 3P excitation (green). Third harmonic generation (THG) imaging visualizes the tracheal arbors (yellow). Arrows indicate different CC compartments that are identified (scale bars= 30µm). (**F-G**) Lateral resolution measurements in 3P images captured at 56µm depth. **(F)** The GFP fluorescence profile of CC ring neurons (green) and **(G)** the THG profile of surrounding trachea (yellow). Lateral intensity profiles measured along the white lines are fitted by Gaussian profiles for the lateral resolution estimation (scale bars=20µm).

Figure 4. Cuticle-removed and cuticle-intact imaging of neural activity across the entire fly brain in response to electric shock. (A-B) 3P imaging of neural activity of the fly brain neuropil at indicated depths using **(A)** the cuticle-intact and **(B)** the cuticle-removed imaging preparations upon 1s electrical stimulation. (**C-D)** 2P imaging of neural activity of the fly brain neuropil at indicated depths using **(C)** the cuticle-intact and **(D)** the cuticle-removed imaging preparations upon 1s electrical stimulation. The cross-section images at different depths are shown on the left (Scale bar = 50 μm). Activity traces within the ROIs enclosed by dotted white lines are shown on the right. Gray lines show the traces of individual stimulations and green lines show the traces of an average of three stimulations. Images were captured at 256x128 pixels/frame and 6.5 Hz frame rate for 3P and 113 Hz frame rate for 2P. 3P and 2P data were averaged to 1.1 Hz effective sampling rate for plotting.

Figure 5. Simultaneous 2P and 3P functional imaging of short-term odor-evoked responses of the mushroom body Kenyon cells.

(A) Schematic of the custom made olfactometer and the through-cuticle functional imaging setup. (**B)** Picture of the head-fixed fly on the ball under the multiphoton microscope. (**C)** Stimulus timeline. The same stimulus scheme was repeated 5 times using the same odor. (**D)** Schematic of the mushroom body anatomy indicating the locations of α, β, and γ lobes. **(E)** γ-lobes have discrete anatomical compartments (shown as γ2–γ5). **(F)** GCaMP6s is expressed in the mushroom body Kenyon cells. Normalized ($\Delta F/F_0$) GCaMP6s signal is shown before (left) and after (right) odor stimulus (scale bar= 20 μm). **(G)** Odor-evoked responses of Kenyon cells captured by 2P excitation at 920 nm and **(H)** 3P excitation at 1320 nm. **(I)** Comparison of the average responses captured by simultaneous 2P and 3P imaging over time (n=3 flies, 4-5 trials per fly, data are presented as mean ± SEM in (**G)** and (**H),** grey bar indicates when stimulus is present). Average laser powers are 5 mW at 920 nm and 4 mW at 1320 nm. Images were captured at 160x165 pixels/frame and 13.2 Hz frame rate. 2P and 3P data were averaged to 6.8 Hz effective sampling rate for plotting.

Figure 6. 2P functional imaging of odor-evoked responses in walking flies.

(A) Schematic of the custom-made odor delivery and spherical treadmill system. (**B)** Odor evoked response in mushroom body γ4 compartment is overlaid with the rotational speed (Sr) measured at the same time. **(C)** Normalized ($\Delta F/F_0$) GCaMP6s signal is shown during the odor stimulation experiments. Odor-evoked responses of Kenyon cells are captured by 2P excitation at 920 nm (n=3 flies, 3 trials per fly, data are presented as mean ± SEM). (**D)** Schematics showing measurements of the rotational and forward speed of flies on the spherical treadmill. (**E-G**) Representative plots for a single fly during the odor stimulation experiments showing rotational speed (Sr) (**E**), forward speed (Sf) (**F**) as a function of time, and the total calculated 2D fictive path (**G**). (**H-K**) Summary heatmap plots and statistical comparison for rotational (**H-I**) and forward speed (**J-K**) 5 seconds before and after the odor stimulation (n=3 flies, 3 trials per fly, paired-two tail t-test, p=0.0225). Average laser power at 920 nm is <10mW**.** Images were captured at 256x128 pixels/frame and 17 Hz frame rate. 2P data were averaged to 5 Hz effective sampling rate for plotting.

Figure 7. Long-term 2P imaging of odor-evoked responses of the mushroom body γ-lobes

(A) Stimulus timeline for long-term odor imaging. GCaMP6s fluorescence signal is captured from Kenyon cells axons innervating mushroom body γ-lobes using the semi-compressed preparation. (**B-E)** Quantification of the normalized signal ($\Delta F/F_0$) over time in each γ-lobe compartment. Light orange bar indicates when the odor stimulus is present. Each colored line indicates the average response of a fly over multiple trials in a given hour. The average response of 3 flies is shown. Each compartment's response is labelled with a different color. **(F)** Quantification of the peak amplitude across different time points and lobes (dF/F_0) (Two-way repeated measures ANOVA. Data are presented as mean ± SEM, ns= not significant, n=3 flies, 3 trials per time point). Average laser power at 920 nm is <10mW. Images were captured at 256x128 pixels/frame and 17 Hz frame rate. 2P data were averaged to 5 Hz effective sampling rate for plotting.

Figure Supplements

Figure 2– figure supplement 1. Head compression does not affect male courtship and removal of air sacs allows 2P and 3P imaging in a head-uncompressed preparation.

(A) Male copulation percentage is quantified in controls and flies that were previously head-compressed (n=7-8, Log-rank (Mantel-Cox) test, $p>0.05$). **(B-D)** Cross section imaging of the mushroom body (MB) Kenyon cells expressing GCaMP6s through the head cuticle at 920 nm (2P) and 1320 nm (3P) excitation after removing air sacs on one side of the head. The fly head is not compressed to the cover slip. The Z projections of **(B)** 2P (cyan) and **(C, D)** 3P (green) imaging stacks. For each imaging preparation, the same fly brain is imaged with 3P excitation and 2P excitation. Mushroom body structures are visible on the side where air sacs are removed. The dotted lines show the area where the air sacs block imaging. **(C)** Zoomed-in 3P image taken from the side of the brain where the air sacs are removed. Mushroom body lobes and the peduncle are clearly visible in the air sac removed side without head compression (Scale bars = 20μm).

Figure 3– figure supplement 1. Comparing fluorescent signal attenuation with 2P and 3P excitation in cuticle-intact and cuticle-removed imaging preparations.

(A-B) Structural cross section images through (A) a cuticle-intact imaging preparation and (B) a cuticle-removed preparation 2P fluorescence (top), 3P fluorescence (middle) and THG (bottom). Flies expressing membrane targeted GFP pan neuronally is used in all experiments. The excitation power for 3P imaging is <15mW, and the repetition rate is 333kHz. The excitation power for 2P imaging is <15mW, and the repetition rate is 80MHz. Scale bars = 50µm. **(C-D)** Normalized signal attenuation with 920nm 2P and 1320 nm 3P excitation in a cuticle-intact (C) and a cuticle-removed (D) fly brain.

Figure 3– figure supplement 2. Structural Imaging of central complex using the cuticle-intact and cuticle-removed imaging preparations.

(A, C) The Z-projection images of the Central complex (left, scale bar=50µm) and zoomed-in images of Ellipsoid body ring neurons (right, scale bar=10 µm) obtained by 3P excitation (A) through the cuticle and (C) after removing the cuticle. Measurements of the axial resolution were taken at the locations indicated by the yellow line. **(B, D)** Axial intensity line profile and its full width at half maximum (FWHM) are shown. **(E, G)** The Z-projection images of the Central complex neuropil (left, scale bar=50µm) and zoomed-in images of Ellipsoid body ring neurons (right, scale bar=10 µm) obtained by 2P excitation (E) through the cuticle and (G) after removing the cuticle. Measurements of the axial resolution were taken at the locations indicated by the yellow line. **(F, H)** Axial intensity line profile and its full width at half maximum (FWHM) are shown. The axial resolution of the 2P and 3P microscope is measured with 0.5-µm diameter fluorescent beads (shown in grey in the axial intensity line profiles). Axial intensity line profile of the location is fitted with a Lorentzian profile to the power of 2 and 3 for 2P and 3P excitation, respectively. Color bar shows the structure of the central complex at different imaging depths.

Figure 3– figure supplement 3. Structural Imaging of mushroom body neurons using the cuticle-intact and cuticle-removed imaging preparations.

(A, C) The Z-projection images of the mushroom body (left, scale bar=50μm) and zoomed-in in images of Kenyon cell bodies (right, scale bar=10 μm) obtained by 3P excitation captured **(A)** through the cuticle and **(C)** after removing the cuticle. Measurements of the axial resolution were taken at the locations indicated by the yellow line. **(B, D)** Axial intensity line profile and its full width at half maximum (FWHM) are shown. **(E, G)** The Z-projection images of the mushroom body (left, scale bar=50μm) and zoomed-in images of Kenyon cells (right, scale bar=10 μm) obtained by 2P excitation captured **(E)** through the cuticle and **(G)** after removing the cuticle. Measurements of the axial resolution were taken at the locations indicated by the yellow line. **(F, H)** Axial intensity line profile and its full width at half maximum (FWHM) are shown. The axial resolution of the 2P and 3P microscope is measured with 0.5-μm diameter fluorescent beads (shown in grey in the axial intensity line profiles). Axial intensity line profile of the location is fitted with a Lorentzian profile to the power of 2 and 3 for 2P and 3P excitation, respectively. Color bar shows the structure of the mushroom body at different imaging depths.

Figure 3– figure supplement 4. Motion analysis during through-cuticle imaging.

(A) Imaging setup. Fly is head-fixed under the microscope objective, walking on a spherical treadmill. **(B)** Cross section images of ellipsoid body ring neurons (Scale bar=20 μm). A single neuron's cell body is selected as an ROI and used for motion measurements (yellow and red circles). **(C)** Absolute movement distance is shown in blue. **(D)** The relative intensity change of a neuron, indicated as a yellow circle, is shown in orange (RMS=root mean square).

Figure 4– figure supplement 1. HSP70 staining of fly brains after 2P and 3P imaging.

(A-B) Representative images of fly brains before and after heat shock. **(A)** Without heat shock, there is minimal HSP70 protein expressed in the fly brain. **(B)** When flies are exposed to heat shock (30^{o}C) for 10 minutes, the HSP70 protein expression is significantly elevated across the brain. (**C)**

Flies head-fixed/compressed but not exposed to laser show no HSP70 expression. **(D-E)**, HSP70 protein expression in the fly brain after (D) 2P or (E) 3P excitation at indicated wavelengths and durations. No obvious change in HSP70 protein expression is observed at 15mW. (**F)** HSP70 protein expression is significantly elevated when flies are exposed to 3P excitation above >25mW for 10 minutes (Scale bars = 50µm, (n=2-4 flies per condition). Laser power is measured after the microscope objective lens using a power meter.

Figure 5– figure supplement 1. Single trial neural activity traces of odor-evoked responses in the mushroom body gamma5 lobes.

(A) Odor-evoked responses of mushroom body gamma5 lobe captured by 2P excitation at 920 nm. Normalized ($\Delta F/F_0$) GCaMP6s signal is shown for three consecutive trials. (**B)** Odor-evoked responses of mushroom body gamma5 lobe captured by 3P excitation at 1320 nm. Normalized ($\Delta F/F_0$) GCaMP6s signal is shown for three consecutive trials. Grey bar indicates when odor stimulus is present. Images were captured at 160x165 pixels/frame and 13.2 Hz frame rate. 2P and 3P data were averaged to 6.8 Hz effective sampling rate for plotting.

Figure 5– figure supplement 2. Neural activity traces from individual Kenyon cell bodies.

(A) Structural images of the Kenyon cell bodies and ROI selection. (B) Quantification of the normalized $\Delta F/F_0$ signal over time in 5 ROIs representing 5 Kenyon cells imaged with 3P excitation through the intact cuticle. Grey bar indicates when the odor stimulus is present (scale bars= 10µm).

VIDEO LEGENDS

Video 1: Video demonstrating how to prepare flies for cuticle-through imaging.

Video 2: Z stack of the mushroom body (MB) Kenyon cells expressing GCaMP6s. Imaging is done through the head cuticle using 1320 nm (3P) excitation after removing air sacs only on one side of the head (scale bar = 50µm, no head compression).

Video 3: Z stack of the ellipsoid body (EB) ring neurons expressing CD8-GFP. Imaging through the head cuticle at 1320 nm (3P) excitation (scale bar=20µm, semi-compressed preparation).

Video 4: T stack of the ellipsoid body (EB) ring neurons expressing CD8-GFP. Imaging through the intact head cuticle at 1320 nm (3P) excitation (scale bar=20µm, air-sac removed preparation).

Video 5: Short term 2P imaging of mushroom body gamma lobe neural activity captured through the intact fly head cuticle during walking and odor exposure. Functional imaging is performed in walking flies during a food odor stimulation (apple cider vinegar) with 2P excitation at 920 nm (semi-compressed preparation, scale bar=50µm). Video is 5X speed up.

Video 6: Chronic 2P imaging of mushroom body gamma lobe neural activity captured through the intact fly head cuticle during odor exposure. Chronic Functional imaging is performed during a food odor stimulation (apple cider vinegar) with 2P excitation at 920 nm (semi-compressed preparation, scale bar=50µm). Video is 10X speed up.

SOURCE DATA LEGENDS

Figure_1_source_data_1.

Source data for plots Figure 1D and 1G.

Figure_3_source_data_1.

Source data for plots Figure 3B and 3C.

Figure_3-figure_supplement 1_source_data_1.

Source data for plots for Figure 3-Supp 1C, D.

Figure_3-figure_supplement 2_source_data_1.

Source data for plots for Figure 3-Supp 2B-H.

Figure_3-figure_supplement 3_source_data_1.

Source data for plots for Figure 3-Supp 3B-H.

Figure_3-figure_supplement 4_source_data.

Source data for plots for Figure 4-Supp 4C, D.

Figure_4_source_data_1.

Source data for plots for Figure 4A-D.

Figure_5_source_data_1,

Source data for plots Figure 5G-5I.

Figure_6_source_data_1.

Source data for plots Figure 6B and 6C.

Figure_6_source_data_2.

Source data for plots Figure 6E-6K.

Figure_7_source_data_1-4.

Source data for plots Figure 7B-7E.

Figure_7_source_data_1_5.

Source data for plot Figure 7F.

MATERIALS AND METHODS

Key Resources Table				
Reagent type (species) or resource	**Designation**	**Source or reference**	**Identifiers**	**Additional information**
Genetic reagent (*D. melanogaster*)	*Mef2-GAL4*	Bloomington Drosophila Stock Center	BDSC: 50742	
Genetic reagent (*D. melanogaster*)	*GMR15B07-GAL4*	Bloomington Drosophila Stock Center	BDSC: 48678	
Genetic reagent (*D. melanogaster*)	*GMR57C10-GAL4*	Bloomington Drosophila Stock Center	BDSC: 39171	
Genetic reagent (*D. melanogaster*)	*10XUAS-IVS-mCD8-GFP*	Bloomington Drosophila Stock Center	BDSC: 32186	
Genetic reagent (*D. melanogaster*)	*20XUAS-IVS-GCaMP6s*	Bloomington Drosophila Stock Center	BDSC: 42746	
Antibody	anti-GFP (Rabbit polyclonal)	Torrey Pines	TP40	IF (1:1000)
Antibody	anti-HSP70 (Rat monoclonal)	Sigma	SAB5200204	IF (1:200)
Antibody	anti-BRP (Mouse monoclonal)	DSHB	nc82	IF (1:20)
Antibody	DyLight 488 (Goat polyclonal anti-Rabbit)	Invitrogen	35552	IF (1:1000)
Antibody	AlexaFluor 546 (Goat polyclonal anti-Rat)	Invitrogen	A-11081	IF (1:1000)
Antibody	AlexaFluor 633 (Goat polyclonal anti-Mouse)	Invitrogen	A-21052	IF (1:250)
Other	PBS	Lonza BioWhittaker	#17-517Q	
Other	Vectashield	Vector Labs	#H-1000-10	

Fly stocks:

Flies were maintained on conventional cornmeal-agar-molasses medium at 23-25°C and 60-70% relative humidity, under a 12hr light: 12hr dark cycle (lights on at 9 A.M.).

Figure 1

Males, w^{1118}/Y; 20XUAS-IVS-GCaMP6s; Mef2-GAL4.

Figure 2

Males, w^{1118}/Y; 10XUAS-IVS-mCD8-GFP; Mef2-GAL4.

Figure 2- figure supplement 1

Panel A: *Females and Males, Canton-S.*

Panel B-D: *Males, w^{1118}/Y; 20XUAS-IVS-GCaMP6s; Mef2-GAL4.*

Figure 3

Panel A-D: *Males, w^{1118}/Y; 10XUAS-IVS-mCD8-GFP; GMR57C10.*

Panel E-G: *Males, w^{1118}/Y; 10XUAS-IVS-mCD8-GFP; GMR15B07-GAL4.*

Figure 3- figure supplement 1

Males, w^{1118}/Y; 10XUAS-IVS-mCD8-GFP; GMR57C10-GAL4.

Figure 3- figure supplement 2

Males, w^{1118}/Y; 10XUAS-IVS-mCD8-GFP; GMR15B07-GAL4.

Figure 3- figure supplement 3

Males, w^{1118}/Y; 10XUAS-IVS-mCD8-GFP; Mef2-GAL4.

Figure 3- figure supplement 4

Males, w^{1118}/Y; 10XUAS-IVS-mCD8-GFP; GMR15B07-GAL4.

Figure 4

Males, w^{1118}/Y; 20XUAS-IVS-GCaMP6s; GMR57C10-GAL4.

Figure 4- figure supplement 1

Panel A, B, F: Males, w^{1118}/Y; 20XUAS-IVS-GCaMP6s; Mef2-GAL4.

Panel C-E: Males, w^{1118}/Y; 10XUAS-IVS-mCD8-GFP; Mef2-GAL4.

Figure 5-7, Figure 5- figure supplement 1-2

Males, w^{1118}/Y; 20XUAS-IVS-GCaMP6s; Mef2-GAL4.

Optical transmission measurements of the fly head cuticle

The measurement setup and procedures are similar to our previous work (Mok et al., 2022). Drosophila cuticle was dissected from the dorsal head capsule of flies that are age and gender controlled (male, 5 days old). The dissected cuticle was sandwiched between two #1 coverslips (VWR #1 16004-094) with ~10 µL of UV curable resin (Bondic UV glue #SK8024) to avoid dehydration of the sample (Figure 1A). Measurements from each dissected cuticle was done within a day. The first several measurements were repeated at the end of all measurements to ensure that dehydration or protein degradation, which may affect the optical properties of the tissue, did not happen as the experiment progressed. The total transmission and ballistic transmission of cuticle samples were measured using a custom-built device (Figure 1B). For ballistic transmission experiments, light from a single-mode fiber was magnified and focused on the cuticle with a ~25µm spot size. We assume that collimated light passes through the sample since the Rayleigh range for a 25µm ($1/e^2$) focus spot is approximately 0.8–1.3 mm in water (refractive index ~ 1.33) for wavelengths between 852 nm and 1624 nm, which is much larger than the thickness of the entire coverslip sandwich-preparation (<400µm). The transmitted light from the cuticle was then coupled to another single-mode fiber with identical focusing optics and detected with a power meter (S146C, Thorlabs). Such a confocal setup ensures that only the ballistic transmission is measured. The incident power is ~10mW on the cuticle for each measurement. An InGaAs camera (WiDy SWIR 640U-S, NiT) and a CMOS camera (DCC1645C, Thorlabs) were used to image the sample and incident beam to ensure that the incident light spot is always on the cuticle and to avoid the dark pigments (usually at the edge of the cuticle), ocelli, and possible cracks introduced during dissection. The ballistic transmission of the cuticle was then calculated as the power ratio between the ballistic transmissions through the cuticle (PT^{SMF}) and the surrounding areas without the cuticle (PT_0^{SMF}), i.e., a reference transmission through areas containing only the UV curable resin, using the equation below:

$$T_{ballistic} = \frac{PT^{SMF}}{PT_0^{SMF}}$$

For measuring the total transmission, light from a single-mode fiber was magnified and focused on the cuticle with a ~50μm spot size. We again assume that collimated light passes through the sample since the Rayleigh range for a 50μm ($1/e^2$) spot size is 5mm - 10mm for wavelengths between 532 nm and 1624 nm. An integrating sphere power meter (S146C, Thorlabs) is placed immediately after the sample to measure the total transmission. The incident power on the sample is ~10mW. The same cameras were used to visualize the light spot and the cuticle when the integrating sphere is removed. The total transmission of the cuticle was then calculated as the optical power ratio between the transmissions through the cuticle (PT^{IS}) and the reference transmission through areas containing only the UV curable resin (PT_0^{IS}), both measured by the integrating sphere (IS).

$$T_{total} = \frac{PT^{IS}}{PT_0^{IS}}$$

Data in Figure 1D and G are acquired by manually translating the sample orthogonal to the light path. For Figures 1E and H, the samples were translated with a motorized stage to acquire a spatially resolved transmission map. We collected data from several locations for each wavelength (ballistic transmission, n=56 measurements across 5 cuticle samples; total transmission, n=20 measurements across 4 samples). We then calculated the mean and the standard error across all measurements for ballistic or total transmission for the plots shown in Figure 1D and G respectively.

2P/3P imaging preparations

Through-cuticle imaging preparation with head compression: All animals used for imaging experiments were male flies with indicated genotypes kept at 25°C incubators and maintained on conventional cornmeal-agar-molasses medium. Flies used for chronic functional experiments were 2-7 days old, and flies used for short term functional experiments were 1-4 days old. To perform through-cuticle brain imaging, flies were first head-fixed in a 40 mm weigh dish (VWR#76299-236) with a hole made with forceps. A drop of UV curable resin (Liquid plastic welder, Bondic®) was applied to the head and thorax, which was then cured with blue light (~470 nm) and fused to a cover glass. The fly antennae are ensured to be fully exposed after curing. Fly proboscises were

immobilized with blue light curable resin to minimize head motion caused by muscle contractions. Video 1 explains the imaging preparation.

Through-cuticle imaging preparation with air sac removal: The dorsal head air sacs were repositioned to the posterior most portion of the head. This was done by deeply anesthetizing the flies on ice for ~5 minutes. The flies were placed into a modified pipette, allowing their head to stick out of the tip. Dental wax was wrapped around the head stabilizing it to the pipette. A sharpened glass capillary held in a micro manipulator was used to make a small incision just medial to the eye on the dorsal posterior area of the fly's head. A sharpened tungsten needle curved into a micro hook, held in a micro manipulator was inserted into the incision, and run just under the cuticle to hook the dorsal air sac. The hook was pulled to the rear of the head, bringing the air sacs with it. The hook was then manipulated to release the air sac. The procedure was repeated on the other side. The incisions were closed using a very small amount of UV curable resin over the incision site. The flies were then allowed to recover for 24 hours at 25 degrees on type S food. Flies used in Figure 4, Figure 2-figure supplement 1, Figure 3-figure supplement 2, Figure 3-figure supplement 4 went through the air sac removal surgery.

Cuticle-removed imaging preparation: Flies were anesthetized on ice for ~1 min then placed into a holder made from a 0.02mm thick carbon steel sheet with a small hole cut to allow the dorsal thorax and dorsal part of the head to protrude through the sheet. The flies were fixed to the imaging chamber using a UV curable resin (Bondic) around the perimeter of the hole in the sheet. ~500μl of adult artificial hemolymph was placed on the imaging chamber and the head cuticle was removed using a 20-gauge needle to cut along the medial perimeter of the eyes, the dorsal posterior extent of the head between the eyes, and just posterior to the antenna along the front of the head. Any air sacs, fat bodies or trachea on top of the exposed brain were removed with fine forceps.

Multiphoton Excitation source

Whole brain 2P/3P imaging: The 3P excitation source is a wavelength-tunable optical parametric amplifier (NOPA, Spectra-Physics) pumped by a femtosecond laser (Spirit, Spectra-Physics) with a MOPA (Master Oscillator Power Amplifier) architecture. The center wavelength is set at 1320 nm.

An SF11 prism pair (PS853, Thorlabs) is used for dispersion compensation in the system. The laser repetition rate is maintained at 333kHz. The 2P excitation source is a Ti: Sapphire laser centered at 920 nm (Chameleon, Coherent). The laser repetition rate is at 80MHz.

3P imaging: The excitation source is a wavelength-tunable optical parametric amplifier (OPA, Opera-F, Coherent) pumped by a femtosecond laser (Monaco, Coherent) with a MOPA (Master Oscillator Power Amplifier) architecture. The center wavelength is set at 1320 nm. An SF10 prism pair (10SF10, Newport) is used for dispersion compensation in the system.

Simultaneous 2P/3P imaging and 2P imaging: The 3P excitation source is a wavelength-tunable optical parametric amplifier (NOPA, Spectra-Physics) pumped by a femtosecond laser (Spirit, Spectra-Physics) with a MOPA (Master Oscillator Power Amplifier) architecture. The center wavelength is set at 1320 nm. An SF11 prism pair (PS853, Thorlabs) is used for dispersion compensation in the system. The laser repetition rate is maintained at 400kHz. The 2P excitation source is a Ti: Sapphire laser centered at 920 nm (Tsunami, Spectra-Physics). The laser repetition rate is at 80MHz.

Multiphoton microscopes

Whole brain 2P/3P imaging: It is taken with a commercial multiphoton microscope with both 2P and 3P light path (Bergamo II, Thorlabs). A high numerical aperture (NA) water immersion microscope objective (Olympus XLPLN25XWMP2, 25X, NA 1.05) is used. For GFP and THG imaging, fluorescence and THG signals are separated and directed to the detector by a 488 nm dichronic mirror (Di02-R488, Semrock) and 562nm dichronic mirror (FF562-Di03). Then the GFP and THG signals are further filtered by a 525/50 nm band-pass filter (FF03-525/50, Semrock) and 447/60 nm (FF02-447/60, Semrock) band-pass filter, respectively. The signals are finally detected by GaAsP PMTs (PMT2101, Thorlabs).

3P imaging: A scan lens with 36mm focal length (LSM03-BB, Thorlabs) and a tube lens with 200mm focal length are used to conjugate the galvo mirrors to the back aperture of the objective. The same high numerical aperture (NA) water immersion microscope objective (Olympus XLPLN25XWMP2, 25X, NA 1.05) is used. Two detection channels are used to collect the fluorescence signal and the

third harmonic generation (THG) signal by photomultiplier tubes (PMT) with GaAsP photocathode (H7422-40, Hamamatsu). For 3-photon imaging of GFP and GCaMP6s at 1320 nm, fluorescence signal and THG signal were filtered by a 520/60 nm band-pass filter (FF01-520/60-25, Semrock) and a 435/40 nm band-pass filter (FF02-435/40-25, Semrock), respectively. For signal sampling, the PMT current is converted to voltage and low pass filtered (200 kHz) by a transimpedance amplifier (C7319, Hamamatsu). Analog-to-digital conversion is performed by a data acquisition card (NI PCI-6110, National Instruments). ScanImage 5.4-Vidrio Technologies (Pologruto et al., 2003) running on MATLAB (MathWorks) is used to acquire images and control a movable objective microscope (MOM, Sutter Instrument Company).

Simultaneous 2P/3P imaging and 2P imaging: A scan lens (SL50-3P, Thorlabs) and tube lens (TL200-3P, Thorlabs) are used to conjugate the galvo mirrors to the back aperture of the objective. The same objective (Olympus XLPLN25XWMP2, 25X, NA 1.05) is used. Fluorescence signals are detected by photomultiplier tubes (PMT) with GaAsP photocathode (H7422-40, Hamamatsu). For GFP and GCaMP6s imaging, fluorescence signal passes through a 466 nm dichronic mirror (Di02R-466) and filtered by a 520/60 nm band-pass filter (FF01-520/60-25, Semrock). For signal sampling, the PMT current is converted to voltage by a 10-MHz transimpedance amplifier (C9999, Hamamatsu). An additional 1.9-MHz low-pass filter (Minicircuts, BLP-1.9+) was used before digital sampling. Analog-to-digital conversion is performed by a data acquisition card (NI PCI- 6115, National Instruments). ScanImage 3.8 -Vidrio Technologies (Pologruto et al., 2003) running on MATLAB (MathWorks) was used to acquire images.

Temporal multiplexing: Simultaneous imaging with 2P excitation and 3P excitation is achieved by temporal multiplexing of the 920 nm Ti: Sapphire laser and 1,320 nm Spirit-NOPA laser. The setup is similar to the one described in a previous study (Ouzounov et al., 2017). Briefly, two lasers were combined with a 980 nm long pass dichronic mirror (BLP01-980R-25, Semrock) and passed through the same microscope. They were spatially overlapped at the same focal position after the objective with a remote focusing module in the 2P light path. The 920 nm laser was intensity modulated with an electro-optic modulator (EOM), which was controlled by a TTL waveform

generated from a signal generator (33210A, Keysight) that is triggered by the Spirit-NOPA laser. The EOM has high transmission for ~1μs between two adjacent Spirit-NOPA laser pulses that are 2.5μs apart. By recording the waveform from the signal generator and the PMT signal simultaneously, the 2P and 3P excited fluorescence signals can be temporally demultiplexed with postprocessing using a custom MATLAB script.

Pulse energy comparisons to obtain 0.1 photon/pulse: The comparison follows the framework described in our previous work (Wang et al., 2020). In brief, a calibration factor that relates the pixel intensity of the image and the number of detected photons is first acquired by using a photon counter (SR400, Stanford instrument). Then, the brightest 0.25%-pixel values of a frame from the whole brain stack are taken as the fluorescence signal and are converted to number of detected photons. Finally, the pulse energy required to obtain 0.1 photon/pulse can be calculated with measured power on the fly surface. The pulse width of the laser pulse to obtain a signal of 0.1 photon/pulse is normalized to 60fs to account for the difference in pulse width between 3P (~60fs) and 2P (~100fs).

Anatomical imaging for imaging depth, resolution, and motion quantifications

In all comparisons, signal strength and effective NA for 2P and 3P imaging were similar.

Resolution quantifications: During the imaging session, the fly was placed on ice to reduce motion. For the mushroom body, 2P and 3P images were taken with a FOV of 270 x 270 μm with a pixel count of 512x512. The zoomed-in images were taken with a FOV of 75x75 μm with a pixel count of 512 x 512. For the central complex, 2P and 3P images were taken with a FOV of 250 x 126 μm with a pixel count of 512*256. The zoomed in images were taken with a FOV of 50x50 μm with a pixel count of 256x256. A step size of 1 μm was taken for axial resolution measurement.

Motion quantifications: Motion artifact during cuticle-intact in vivo 3P imaging was quantified by imaging ellipsoid body ring neurons expressing GFP. A video of 150s is taken at a frame rate of 6.5Hz with a field-of-view of 74 x 37 μm and pixel count of 256x128. The motion was calculated with the “landmark” output that targets a single neuron from TurboReg plugin in ImageJ during image registration. After image registration, the intensity change of one neuron (I), as indicated in the ROI

(Figure3-figure supplement 4**)**, in time was normalized according to the formula $(I- I_0)/I_0$. I_0 is taken as the mean of all intensity value (I) of the trace.

Whole brain signal attenuation quantification: 2P and 3P image stacks were taken with a FOV 200x 100µm with a pixel count of 512x256. Axial step sizes of 5 and 10 µm were used for cuticle-intact and cuticle-removed fly, respectively. The imaging power was increased with imaging depth to keep the signal level approximately constant. The maximum power on the fly brain was 15mW for both 2P and 3P. The signal (S) of each frame was calculated as the average of the brightest 0.25%-pixel values and then normalized by the imaging power (P) on the fly surface. The normalization was S/P^2 and S/P^3 for the 2P and 3P stacks, respectively. The effective attenuation length (EAL) was then derived by least-squares linear regression of the normalized fluorescence signal at different imaging depth.

Electrical stimulation during 2P/3P functional imaging

Cuticle-removed preparation: A tungsten wire was inserted into the adult artificial hemolymph on top of the exposed fly brain and secured in placed with UV curable resin A copper wire was placed in contact with ventral portion of the body of the fly and secured in place with UV curable resin. The wires were connected to a variable power supply with the tungsten positive side interrupted with a normally open relay module controlled with a micro-controller (Arduino Uno R3).

Cuticle-intact preparation: Flies were prepared as described before for head compression imaging (Supplementary Video1). A 26-gauge copper wire was secured to the glass cover slip next to the head and another copper wire was secured to the ventral portion of the body. Low melting agarose (GeneMate #E-3126-25) with 0.5M NaCl (Sigma #S7653-250G) was used to make an electrical connection between the wires and the fly, making sure the electrical path runs through the body.

Electrical stimulation and imaging: Both the cuticle-intact and cuticle-removed flies were imaged with 2P and 3P excitation, taking images at different depths throughout the brain. For electrical stimulation the flies were stimulated for 1 second at 5 volts and imaged at various depths to see a consistent GCaMP signal increase. Three photon activity was taken with a FOV of 200 x 100 µm with pixel count of 256 x 128. The frame rate was 6.5Hz. Every 5 frames were averaged to achieve

an effective frame rate of 1.3 Hz. 2P activity was taken with a FOV of 200 x 100 µm with pixel count of 256 x 128. The frame rate is 113Hz. Every 100 frames are averaged to achieve an effective frame rate of 1.1Hz. Regions of interest (ROIs) were generated by manual segmentation. The baselines of the activity traces (F0) for each ROIs were determined using a rolling average of 4s over the trace after excluding data points during electric stimulation. The activity traces (F) were normalized according to the formula (F − F0)/F0. Three stimulations were done for each depth.

Olfactory imaging conditions and preparation of flies used in imaging experiments

Simultaneous 2P/3P functional imaging: Flies were food deprived for 16-24 hours in vials with a wet Kim wipe. Each odor stimulation trial consisted of 50 seconds of clean mineral oil, 3 seconds of undiluted apple cider vinegar stimulus, and another 50 seconds of mineral oil. Between trials, scanning was stopped for 20 seconds to minimize the risk of imaging-induced tissue stress. Five trials were performed sequentially. Images were captured at 160x165 pixels/frame and 13.2 Hz frame rate. 2P and 3P data were averaged to 6.8 Hz effective sampling rate for plotting.

2P functional imaging in behaving flies: Flies were head-fixed using a custom 3D-printed apparatus which also holds the tube for odor delivery. In this setup, flies are allowed to walk on a spherical treadmill and turn towards the odor stimuli. The odor stimulus is located on the right side of the fly. Each odor stimulation trial consisted of 60 seconds of clean mineral oil, 3 seconds of undiluted apple cider vinegar stimulus, and another 60 seconds of mineral oil. Every change of odor triggers the acquisition software to save in a new file. The images were captured at 256*128-pixel resolution and 17 Hz frame rate. Three trials were performed sequentially.

2P chronic functional imaging: Flies used in long term functional imaging experiments were kept on regular fly food before the first trial to assure that they were satiated. Each odor stimulation trial consisted of 60 seconds of clean mineral oil, 3 seconds of undiluted apple cider vinegar stimulus, and another 60 seconds of mineral oil. Every change of odor triggers the acquisition software to save in a new file. The images were captured at 256*128-pixel resolution and 17 Hz frame rate. Three trials were performed sequentially, and the three-trial block was repeated every four hours. Between trial blocks, scanning was stopped, and air passing through the stimulation tube was

redirected to the exhaust valve to prevent desiccation. To further prevent desiccation, flies were placed on a water-absorbing polymer bead.

Olfactory Stimulation

Odor delivery during 2P/3P simultaneous functional imaging**:** Food odor, apple cider vinegar, was delivered using a custom built olfactometer as described previously (Raccuglia et al., 2016). Clean room air was pumped (Active Aqua Air Pump, 4 Outlets, 6W, 15 L/min) into the olfactometer, and the flow rate was regulated by a mass flow controller (Aalborg GFC17). Two Arduino controlled 3-way solenoid valves (3-Way Ported Style with Circuit Board Mounts, LFAA0503110H) controlled air flow. One valve delivered the odorized airstream either to an exhaust outlet or to the main air channel, while another valve directed air flow either to the stimulus or control channel. The stimulus channel contained a 50 ml glass vial containing undiluted apple cider vinegar (volume=10 ml) (Wegmans), while the control channel contained a 50 ml glass vial containing mineral oil (volume=10 ml). Flies were placed approximately 1 cm from a clear PVC output tube (OD = 1.3 mm, ID = 0.84 mm), which passed a ~1< L/min air stream to the antennae. The odor stimulus latency was calculated before the experiments using a photo ionization detector (PID) (Aurora Scientific). We sampled odor delivery using the PID every 20ms and found average latency to peak odor amplitude was < 100ms across 34 measurements. Flies were stimulated with air (50s), before and after the odor stimulus (odor + air, 3s). Same stimulus scheme was repeated 3 times.

Odor delivery during spherical treadmill and chronic imaging**:** An air supported spherical treadmill setup was used to record fly walking behavior during multiphoton imaging. Male flies at 5-6 days post eclosion were anesthetized on ice for about 2 minutes and mounted to a coverslip with semi-compression as described in Video 1. The cover slip was glued to a custom 3D printed holder with an internal airway to deliver airflow along the underside of the coverslip directly onto the antenna without interfering with the air supported ball. The air duct was positioned 90 degrees to the right of the fly about 1cm away. Clean room air was pumped (Hygger B07Y8CHXTL) into a mass flow meter set at 1L/min (Aalborg GFC17). The regulated airflow was directed through an Arduino controlled three-way solenoid pinch valve (Masterflex UX-98302-42) using 1/16” ID tubing. The

valve directed the airflow either through 50ml glass vile containing 10ml of undiluted apple cider vinegar for the stimulus, or through a 50ml glass vile containing 10ml of mineral oil for the control. The latency from stimulus signal from the Arduino to odor molecules arriving at the fly's antenna was measured using a photo-ionization detector (Aurora Scientific) prior to the experiments and found to be <200ms to peak stimulus.

Fly behavior during olfactory stimulation coupled with 2P/3P imaging

The spherical treadmill was manufactured by custom milling with 6061 aluminum alloy. The treadmill has a concave surface at the end for placing the ball, which is supported by airflow. We fabricated foam balls (Last-A-Foam FR-7110, General Plastics, Burlington Way, WA USA) that are 10mm in diameter using a ball-shaped file. We drew random patterns with black ink on the foam balls to provide a high-contrast surface for the ball tracking analysis. Fly behavior was videotaped from the side to capture any movement by a CCD camera (DCC1545M, Thorlabs) equipped with a machine vision camera lens (MVL6X12Z, Thorlabs) and 950 nm long pass filter (FELH0950, Thorlabs). The acquisition frame rate for video recording was set to 8Hz under IR light illumination at 970 nm (M970L4, Thorlabs). The stimulus signal from the Arduino is captured by NI-6009 (National Instrument) using a custom script written in MATLAB 2020b (Mathworks) to synchronize with the behavior video in data analysis.

Male courtship assay

5-6 days of wildtype virgin female and male flies were collected right after eclosion and aged at 25^{o}C for ~5 days. On the day of the courtship assay, control group males were placed on ice for 1-5 minutes, then placed in the imaging chamber without being head-compressed or head-fixed. They were allowed to recover for 5 hours at 25^{o}C before getting tested in the courtship assay. Experimental group flies went through the entire head compression and head-fixing procedure described in Video 1. These flies were removed from the imaging chamber after being head-fixed and allowed to recover for 5 hours at 25^{o}C before getting tested in the courtship assay. To quantify male courtship behavior, male and female flies were aspirated into a 1cm courtship chamber and

allowed to interact for 30 minutes. Courtship assays were recorded using a camera (FLIR Blackfly, BFS-U3-31S4M-C).

Immunohistochemistry for brain tissue damage assessment

To investigate laser-induced stress in the fly brain, we exposed 4-6-day old male flies (MB>UAS-GFP) to 2P laser at 920nm with 15mW power or to a 3P laser at 1320nm with 15mW power. Flies were prepared using the medium compression preparation described previously. Control flies were prepared the same way and kept in the dark at room temperature for the duration of the experimental procedure. Laser scanning was done in the same depth as the MB gamma lobes. Each scan lasted for six minutes. Flies were rested for six minutes until the next imaging session. Each fly was exposed to four imaging sessions. Once the experiment was completed, fly brains were dissected and stained with the HSP70 antibody. For the positive control group, flies were exposed to 30^{o}C for 10 minutes in an incubator to induce HSP70 expression. For the negative control group, flies were kept at room temperature. Brains from each experimental and control groups were dissected in phosphate-buffered saline (PBS) and incubated in 4% paraformaldehyde (PFA) in PBS for 20-30 minutes at room temperature on an orbital shaker. Tissues were washed 3-4 times over 1 hour in PBS (calcium- and magnesium-free; Lonza BioWhittaker #17-517Q) containing 0.1% Triton X-100 (PBT) at room temperature. Samples were blocked in 5% Normal Goat Serum in PBT (NGS-PBT) for 1 hour and then incubated with primary antibodies diluted in NGS-PBT for 24 hours at 4^{o}C. Primary antibodies used were anti-GFP (Torrey Pines, TP40, rabbit polyclonal, 1:1000), anti-BRP (DSHB, nc82, mouse monoclonal, 1:20), and anti-HSP70 (Sigma, SAB5200204, rat monoclonal, 1:200). The next day, samples were washed 5-6 times over 2 hours in PBT at room temperature and incubated with secondary antibodies (Invitrogen) diluted in NGS-PBT for 24 hours at 4^{o}C. On the third day, samples were washed 4-6 times over 2 hours in PBT at room temperature and mounted with VECTASHIELD Mounting Media (Vector Labs, Burlingame, CA, USA) using glass slides between two bridge glass coverslips. The samples were covered by a glass coverslip on top and sealed using clear nail polish. Images were acquired at 1024x1024 pixel resolution at ~1.7 μm intervals using an upright Zeiss LSM 880 laser scanning confocal microscope

and Zeiss digital image processing software ZEN. The power, pinhole size and gain values were kept the same for all imaged brains during confocal microscopy.

Image processing and data analysis

Resolution measurements: We measured the lateral or axial brightness distribution of small features within the fly brains using either the GFP fluorescence signal (Figure 3F) or the THG signal (Figure 3D and G). Lateral intensity profiles measured along the white lines were fitted by a Gaussian profile for the estimation of the lateral resolution. Axial intensity profiles measured were fitted with a Lorentzian profile to the power of 2 or 3 for 3P and 2P respectively. The full-width half maximum (FWHM) of the profiles were shown in the figures.

Measurement of excitation light attenuation in the fly brain: The image stack was taken with 5 μm step size in depth, and the imaging power was increased with imaging depth to keep the signal level approximately constant. The signal (S) of each frame was calculated as the average of the brightest 0.25%-pixel values and then normalized by the imaging power (P) on the fly surface. The normalization is S/P^2 and S/P^3 for the 2P and 3P stacks, respectively. The effective attenuation length (EAL) is then derived by least-squares linear regression of the normalized fluorescence or THG signal at different imaging depth (Figure 3B and C).

Image processing for structural imaging. TIFF stacks containing fluorescence and THG data were processed using Fiji, an open-source platform for biological-image analysis (Schindelin et al., 2012). When necessary, stacks were registered using the TurboReg plugin.

Multiplex 2P and 3P functional imaging: TIFF stacks containing fluorescence data were converted to 32 bits, and pixel values were left unscaled. Lateral movement of the sample in the image series, if any, was corrected by TurboReg plug-in in ImageJ. Images acquired during the multiplexed 2P-3P imaging sessions were first median filtered with a filter radius of 10 pixels to reduce high amplitude noise. To compute $\Delta F/F_0$ traces, γ-lobe ROIs were first manually selected using a custom Python script. F_0 was computed as the average of 10 frames preceding stimulus onset. The F_0 image was then subtracted from each frame, and the resulting image was divided by F_0. The resulting trace was then low pass filtered by a moving mean filter with a window size of 8 frames. Data were

analyzed using Python and plotted in Microsoft Excel. Peak $\Delta F/F_0$ was determined by the peak value within 20 frames after the odor delivery.

2P functional imaging in behaving flies and chronic functional imaging: Lateral movement of the sample in the image series, if any, was corrected by TurboReg plug-in in ImageJ. A custom script written in MATLAB 2016b is used for all subsequent processing. Every 4 frames are averaged to achieve an effective frame rate of 4.25 Hz. Regions of interest (ROIs) were generated by manual segmentation of the mushroom bodies. The baselines of the activity traces (F0) for each ROIs are determined using a rolling average of 4s over the trace after excluding data points during odor stimulation. The activity traces (F) were normalized according to the formula $(F - F_0)/F_0$. The trace is finally resampled to 5Hz with spline interpolation to compile with the timing in the motion tracking trace.

Fly walking behavior analysis: Fly walking traces were obtained using the FicTrac (Fictive path Tracking) software as published previously (Moore et al., 2014). The ball rotation analysis was performed using the 'sphere_map_fn' function, which allows the use of a previously generated map of the ball to increase tracking accuracy. We post-processed the raw output generated by FicTrac. To calculate forward and rotational speeds, we used the delta rotation vectors for each axis. Then, we down-sampled raw data from 8Hz to 5Hz by averaging the values in the 200ms time-windows. The empty data points generated from down-sampling were linearly interpolated.

Male courtship behavior analysis: The courtship videos were scored manually, and the time of copulation was recorded per each pair.

Statistics

Sample sizes used in this study were based on previous literature in the field. Experimenters were not blinded in most conditions as almost all data analysis were automated and done using a standardized computer code. All statistical analysis was performed using Prism 9 Software (GraphPad, version 9.0.2). Comparisons with one variable were first analyzed using one-way ANOVA followed by Tukey's multiple comparisons post-hoc test. Comparisons with more than one variable were first analyzed using two-way ANOVA. Comparisons with repeated measures were

analyzed using a paired t-test. We used pair-wise Log-rank (Mantel-Cox) test to compare the copulation percentage curves in the male courtship assays. P values are indicated as follows: ****p < 0.0001; ***p < 0.001; **p < 0.01; and *p < 0.05. Plots labeled with different letters in each panel are significantly different from each other.

Data availability

All data supporting the findings of this study is included in the paper and the supplemental files.

Competing financial interests

The authors declare no competing financial interests.

REFERENCES

Akbari, N., Rebec, M.R., Xia, F., and Xu, C. (2022). Imaging deeper than the transport mean free path with multiphoton microscopy. Biomed Opt Express *13*, 452-463.

Alvarez-Salvado, E., Licata, A.M., Connor, E.G., McHugh, M.K., King, B.M., Stavropoulos, N., Victor, J.D., Crimaldi, J.P., and Nagel, K.I. (2018). Elementary sensory-motor transformations underlying olfactory navigation in walking fruit-flies. Elife *7:e37815*.

Barron, A.B., Gurney, K.N., Meah, L.F., Vasilaki, E., and Marshall, J.A. (2015). Decision-making and action selection in insects: inspiration from vertebrate-based theories. Front Behav Neurosci *9*, 216.

Chen, T.W., Wardill, T.J., Sun, Y., Pulver, S.R., Renninger, S.L., Baohan, A., Schreiter, E.R., Kerr, R.A., Orger, M.B., Jayaraman, V.*, et al.* (2013). Ultrasensitive fluorescent proteins for imaging neuronal activity. Nature *499*, 295-300.

Cohn, R., Morantte, I., and Ruta, V. (2015). Coordinated and Compartmentalized Neuromodulation Shapes Sensory Processing in Drosophila. Cell *163*, 1742-1755.

Crittenden, J.R., Skoulakis, E.M., Han, K.A., Kalderon, D., and Davis, R.L. (1998). Tripartite mushroom body architecture revealed by antigenic markers. Learn Mem *5*, 38-51.

Dickson, B.J. (2008). Wired for sex: the neurobiology of Drosophila mating decisions. Science *322*, 904-909.

Dong, C.Y., Koenig, K., and So, P. (2003). Characterizing point spread functions of two-photon fluorescence microscopy in turbid medium. J Biomed Opt *8*, 450-459.

Grover, D., Katsuki, T., and Greenspan, R.J. (2016). Flyception: imaging brain activity in freely walking fruit flies. Nat Methods *13*, 569-572.

Hefendehl, J.K., Milford, D., Eicke, D., Wegenast-Braun, B.M., Calhoun, M.E., Grathwohl, S.A., Jucker, M., and Liebig, C. (2012). Repeatable target localization for long-term in vivo imaging of mice with 2-photon microscopy. J Neurosci Methods *205*, 357-363.

Horton, N.G., Wang, K., Kobat, D., Clark, C.G., Wise, F.W., Schaffer, C.B., and Xu, C. (2013). In vivo three-photon microscopy of subcortical structures within an intact mouse brain. Nat Photonics *7*, 205–209.

Huang, C., Maxey, J.R., Sinha, S., Savall, J., Gong, Y., and Schnitzer, M.J. (2018). Long-term optical brain imaging in live adult fruit flies. Nat Commun *9*, 872.

Hunt, L.T., and Hayden, B.Y. (2017). A distributed, hierarchical and recurrent framework for reward-based choice. Nat Rev Neurosci *18*, 172-182.

Ito, K., Suzuki, K., Estes, P., Ramaswami, M., Yamamoto, D., and Strausfeld, N.J. (1998). The organization of extrinsic neurons and their implications in the functional roles of the mushroom bodies in Drosophila melanogaster Meigen. Learn Mem *5*, 52-77.

Ji, N., Freeman, J., and Smith, S.L. (2016). Technologies for imaging neural activity in large volumes. Nat Neurosci *19*, 1154-1164.

Krashes, M.J., Keene, A.C., Leung, B., Armstrong, J.D., and Waddell, S. (2007). Sequential use of mushroom body neuron subsets during drosophila odor memory processing. Neuron *53*, 103-115.

LaViolette, A.K., and Xu, C. (2021). Shot noise limits on binary detection in multiphoton imaging. Biomed Opt Express *12*, 7033-7048.

Lerner, T.N., Ye, L., and Deisseroth, K. (2016). Communication in Neural Circuits: Tools, Opportunities, and Challenges. Cell *164*, 1136-1150.

Lin, S., Senapati, B., and Tsao, C.H. (2019). Neural basis of hunger-driven behaviour in Drosophila. Open Biol *9*, 180259.

Lin, Y.Y., Wu, M.C., Hsiao, P.Y., Chu, L.A., Yang, M.M., Fu, C.C., and Chiang, A.S. (2015). Three-wavelength light control of freely moving Drosophila Melanogaster for less perturbation and efficient social-behavioral studies. Biomed Opt Express *6*, 514-523.

Lindquist, S. (1980). Varying patterns of protein synthesis in Drosophila during heat shock: implications for regulation. Dev Biol *77*, 463-479.

Luo, L., Callaway, E.M., and Svoboda, K. (2018). Genetic Dissection of Neural Circuits: A Decade of Progress. Neuron *98*, 256-281.

Lutcke, H., Margolis, D.J., and Helmchen, F. (2013). Steady or changing? Long-term monitoring of neuronal population activity. Trends Neurosci *36*, 375-384.

Minocci, D., Carbognin, E., Murmu, M.S., and Martin, J.R. (2013). In vivo functional calcium imaging of induced or spontaneous activity in the fly brain using a GFP-apoaequorin-based bioluminescent approach. Biochim Biophys Acta *1833*, 1632-1640.

Mok, A.T., Shea, J., Wu, C., Xia, F., Tatarsky, R., Yapici, N., and Xu, C. (2022). Spatially resolved measurements of ballistic and total transmission in microscale tissue samples from 450 nm to 1624 nm. Biomed Opt Express *13*, 438-451.

Mok, A.T., Wang, T., Xia, F., Wu, C., and Xu, C. (2019). Simultaneous Two- and Three-photon Imaging of Multilayer Neural Activities with Remote Focusing. Paper presented at: Conference on Lasers and Electro-Optics (San Jose, California: Optical Society of America).

Moore, R.J., Taylor, G.J., Paulk, A.C., Pearson, T., van Swinderen, B., and Srinivasan, M.V. (2014). FicTrac: a visual method for tracking spherical motion and generating fictive animal paths. J Neurosci Methods *225*, 106-119.

Ouzounov, D.G., Wang, T., Wang, M., Feng, D.D., Horton, N.G., Cruz-Hernandez, J.C., Cheng, Y.T., Reimer, J., Tolias, A.S., Nishimura, N.*, et al.* (2017). In vivo three-photon imaging of activity of GCaMP6-labeled neurons deep in intact mouse brain. Nat Methods *14*, 388-390.

Owald, D., and Waddell, S. (2015). Olfactory learning skews mushroom body output pathways to steer behavioral choice in Drosophila. Curr Opin Neurobiol *35*, 178-184.

Pfeiffer, K., and Homberg, U. (2014). Organization and functional roles of the central complex in the insect brain. Annu Rev Entomol *59*, 165-184.

Podgorski, K., and Ranganathan, G. (2016). Brain heating induced by near-infrared lasers during multiphoton microscopy. J Neurophysiol *116*, 1012-1023.

Pologruto, T.A., Sabatini, B.L., and Svoboda, K. (2003). ScanImage: flexible software for operating laser scanning microscopes. Biomed Eng Online *2*, 13.

Raccuglia, D., McCurdy, L.Y., Demir, M., Gorur-Shandilya, S., Kunst, M., Emonet, T., and Nitabach, M.N. (2016). Presynaptic GABA Receptors Mediate Temporal Contrast Enhancement in Drosophila Olfactory Sensory Neurons and Modulate Odor-Driven Behavioral Kinetics. eNeuro *3*.

Sayin, S., De Backer, J.-F., Siju, K.P., Wosniack, M.E., Lewis, L.P., Frisch, L.-M., Gansen, B., Schlegel, P., Edmondson-Stait, A., Sharifi, N.*, et al.* (2019). A Neural Circuit Arbitrates between Persistence and Withdrawal in Hungry Drosophila. Neuron *104*, 544-558.e546.

Schindelin, J., Arganda-Carreras, I., Frise, E., Kaynig, V., Longair, M., Pietzsch, T., Preibisch, S., Rueden, C., Saalfeld, S., Schmid, B.*, et al.* (2012). Fiji: an open-source platform for biological-image analysis. Nat Methods *9*, 676-682.

Seelig, J.D., Chiappe, M.E., Lott, G.K., Dutta, A., Osborne, J.E., Reiser, M.B., and Jayaraman, V. (2010). Two-photon calcium imaging from head-fixed Drosophila during optomotor walking behavior. Nat Methods *7*, 535-540.

Seelig, J.D., and Jayaraman, V. (2015). Neural dynamics for landmark orientation and angular path integration. Nature *521*, 186-191.

Simpson, J.H., and Looger, L.L. (2018). Functional Imaging and Optogenetics in Drosophila. Genetics *208*, 1291-1309.

Sinha, S., Liang, L., Ho, E.T., Urbanek, K.E., Luo, L., Baer, T.M., and Schnitzer, M.J. (2013). High-speed laser microsurgery of alert fruit flies for fluorescence imaging of neural activity. Proc Natl Acad Sci U S A *110*, 18374-18379.

Strausfeld, N.J., Hansen, L., Li, Y., Gomez, R.S., and Ito, K. (1998). Evolution, discovery, and interpretations of arthropod mushroom bodies. Learn Mem *5*, 11-37.

Svoboda, K., and Yasuda, R. (2006). Principles of two-photon excitation microscopy and its applications to neuroscience. Neuron *50*, 823-839.

Tao, X., Lin, H.H., Lam, T., Rodriguez, R., Wang, J.W., and Kubby, J. (2017). Transcutical imaging with cellular and subcellular resolution. Biomed Opt Express *8*, 1277-1289.

Tinbergen, N. (1969). The study of instinct (Oxford: Oxford University Press).

Trachtenberg, J.T., Chen, B.E., Knott, G.W., Feng, G., Sanes, J.R., Welker, E., and Svoboda, K. (2002). Long-term in vivo imaging of experience-dependent synaptic plasticity in adult cortex. Nature *420*, 788-794.

Wang, J.W., Wong, A.M., Flores, J., Vosshall, L.B., and Axel, R. (2003). Two-photon calcium imaging reveals an odor-evoked map of activity in the fly brain. Cell *112*, 271-282.

Wang, M., Wu, C., Sinefeld, D., Li, B., Xia, F., and Xu, C. (2018a). Comparing the effective attenuation lengths for long wavelength in vivo imaging of the mouse brain. Biomed Opt Express *9*, 3534-3543.

Wang, T., Ouzounov, D.G., Wu, C., Horton, N.G., Zhang, B., Wu, C.H., Zhang, Y., Schnitzer, M.J., and Xu, C. (2018b). Three-photon imaging of mouse brain structure and function through the intact skull. Nat Methods *15*, 789-792.

Wang, T., Wu, C., Ouzounov, D.G., Gu, W., Xia, F., Kim, M., Yang, X., Warden, M.R., and Xu, C. (2020). Quantitative analysis of 1300-nm three-photon calcium imaging in the mouse brain. Elife *9:e53205*.

Wolff, T., Iyer, N.A., and Rubin, G.M. (2015). Neuroarchitecture and neuroanatomy of the Drosophila central complex: A GAL4-based dissection of protocerebral bridge neurons and circuits. J Comp Neurol *523*, 997-1037.

Xie, X., Tabuchi, M., Brown, M.P., Mitchell, S.P., Wu, M.N., and Kolodkin, A.L. (2017). The laminar organization of the Drosophila ellipsoid body is semaphorin-dependent and prevents the formation of ectopic synaptic connections. Elife *6:e25328*.

Yagi, R., Mabuchi, Y., Mizunami, M., and Tanaka, N.K. (2016). Convergence of multimodal sensory pathways to the mushroom body calyx in Drosophila melanogaster. Sci Rep *6*, 29481.

Yildirim, M., Sugihara, H., So, P.T.C., and Sur, M. (2019). Functional imaging of visual cortical layers and subplate in awake mice with optimized three-photon microscopy. Nat Commun *10*, 177.

Zheng, Z., Lauritzen, J.S., Perlman, E., Robinson, C.G., Nichols, M., Milkie, D., Torrens, O., Price, J., Fisher, C.B., Sharifi, N.*, et al.* (2018). A Complete Electron Microscopy Volume of the Brain of Adult Drosophila melanogaster. Cell *174*, 730-743 e722.

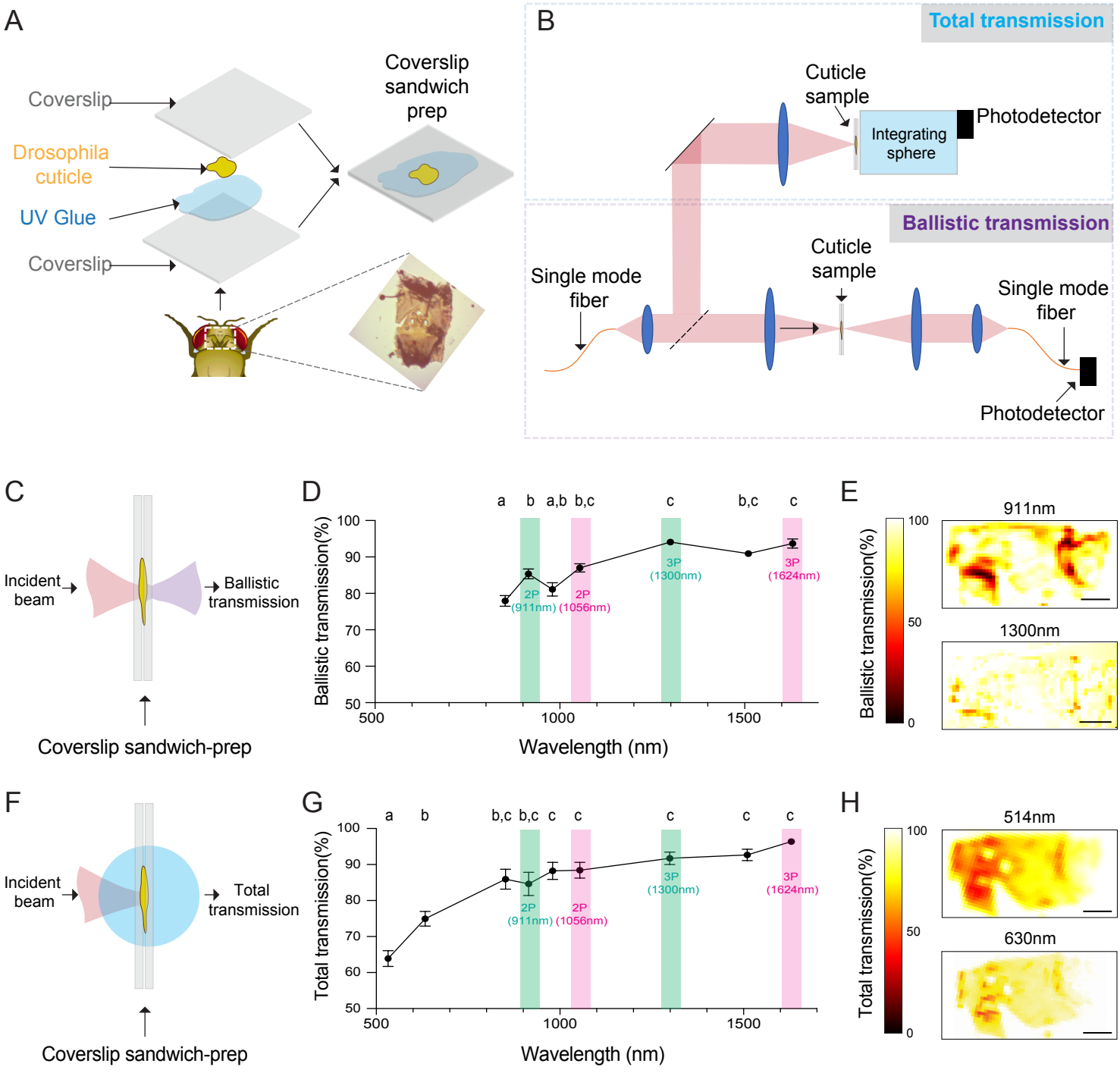
A
Coverslip
Drosophila cuticle
UV Glue
Coverslip
Coverslip sandwich prep
B
Total transmission
Cuticle sample
Integrating sphere
Photodetector
Ballistic transmission
Single mode fiber
Cuticle sample
Single mode fiber
Photodetector
C
Incident beam
Ballistic transmission
Coverslip sandwich-prep
D
Ballistic transmission(%)
Wavelength (nm)
a b a,b b,c c b,c c
2P (911nm)
2P (1056nm)
3P (1300nm)
3P (1624nm)
E
Ballistic transmission(%)
911nm
1300nm
F
Incident beam
Total transmission
Coverslip sandwich-prep
G
Total transmission(%)
Wavelength (nm)
a b b,c b,c c c c c c
2P (911nm)
2P (1056nm)
3P (1300nm)
3P (1624nm)
H
Total transmission(%)
514nm
630nm

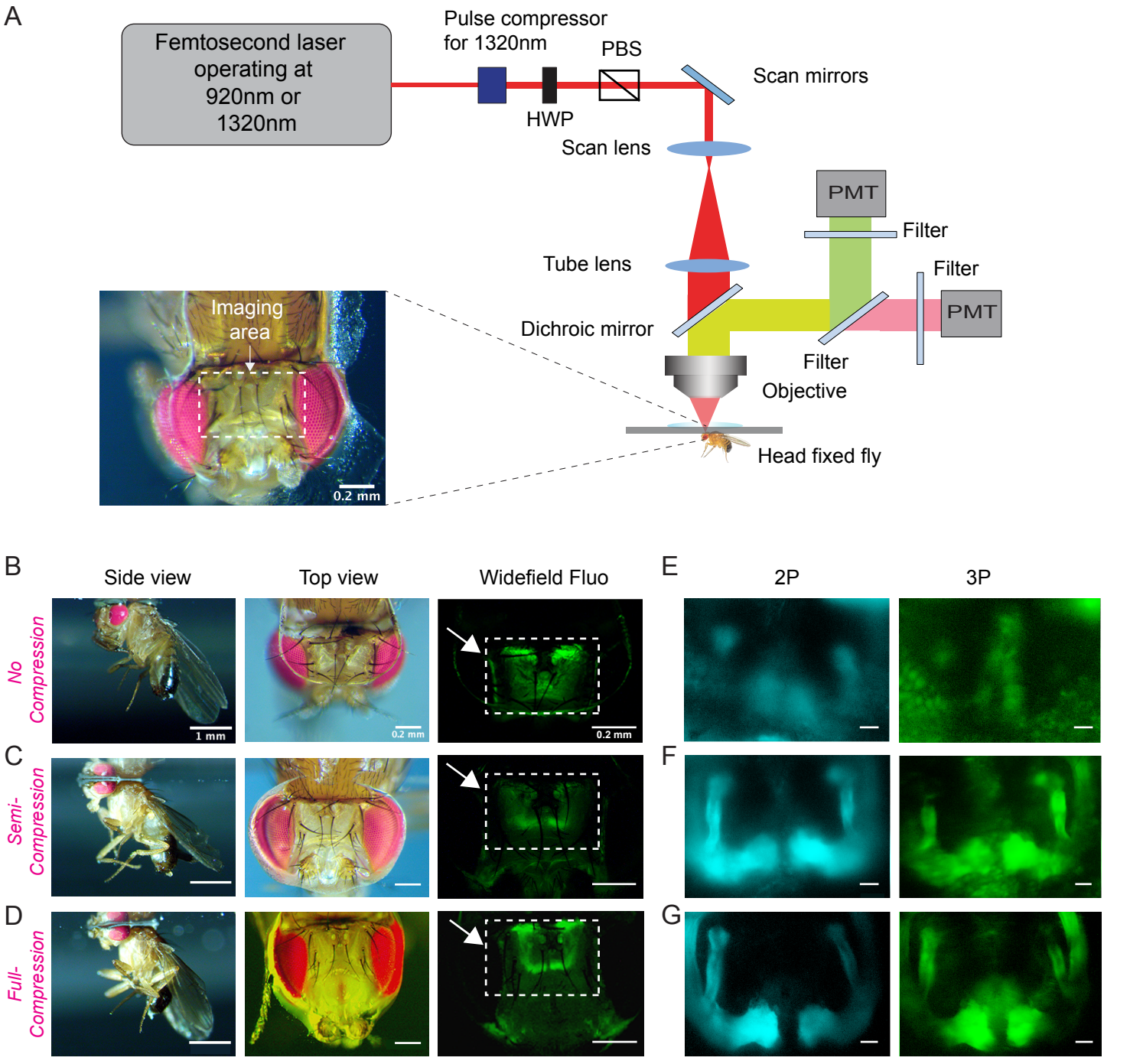
A
Femtosecond laser operating at 920nm or 1320nm
Pulse compressor for 1320nm
PBS
HWP
Scan mirrors
Scan lens
PMT
Filter
Tube lens
Filter
PMT
Dichroic mirror
Filter
Objective
Head fixed fly
Imaging area
0.2 mm
B
Side view
Top view
Widefield Fluo
No Compression
1 mm
0.2 mm
0.2 mm
C
Semi-Compression
D
Full-Compression
E
2P
3P
F
G

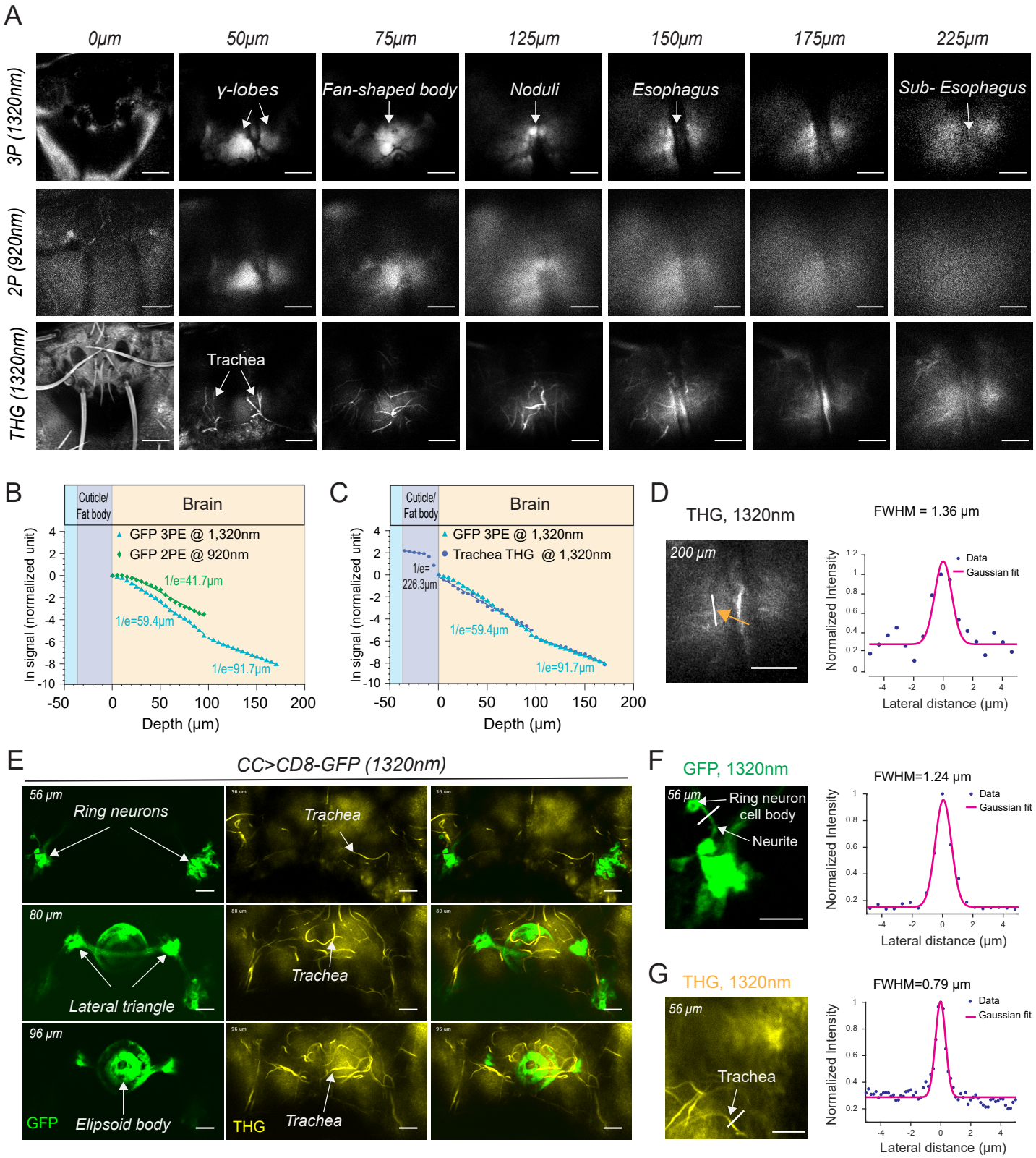
A
0μm
50μm
75μm
125μm
150μm
175μm
225μm
3P (1320nm)
2P (920nm)
THG (1320nm)
γ-lobes
Fan-shaped body
Noduli
Esophagus
Sub- Esophagus
Trachea
B
Cuticle/ Fat body
Brain
GFP 3PE @ 1,320nm
GFP 2PE @ 920nm
1/e=41.7μm
1/e=59.4μm
1/e=91.7μm
ln signal (normalized unit)
Depth (μm)
C
Cuticle/ Fat body
Brain
GFP 3PE @ 1,320nm
Trachea THG @ 1,320nm
1/e= 226.3μm
1/e=59.4μm
1/e=91.7μm
ln signal (normalized unit)
Depth (μm)
D
THG, 1320nm
200 μm
FWHM = 1.36 μm
Data
Gaussian fit
Normalized Intensity
Lateral distance (μm)
E
CC>CD8-GFP (1320nm)
56 μm
Ring neurons
Trachea
80 μm
Lateral triangle
Trachea
96 μm
GFP
Elipsoid body
THG
Trachea
F
GFP, 1320nm
56 μm
Ring neuron cell body
Neurite
FWHM=1.24 μm
Data
Gaussian fit
Normalized Intensity
Lateral distance (μm)
G
THG, 1320nm
56 μm
Trachea
FWHM=0.79 μm
Data
Gaussian fit
Normalized Intensity
Lateral distance (μm)

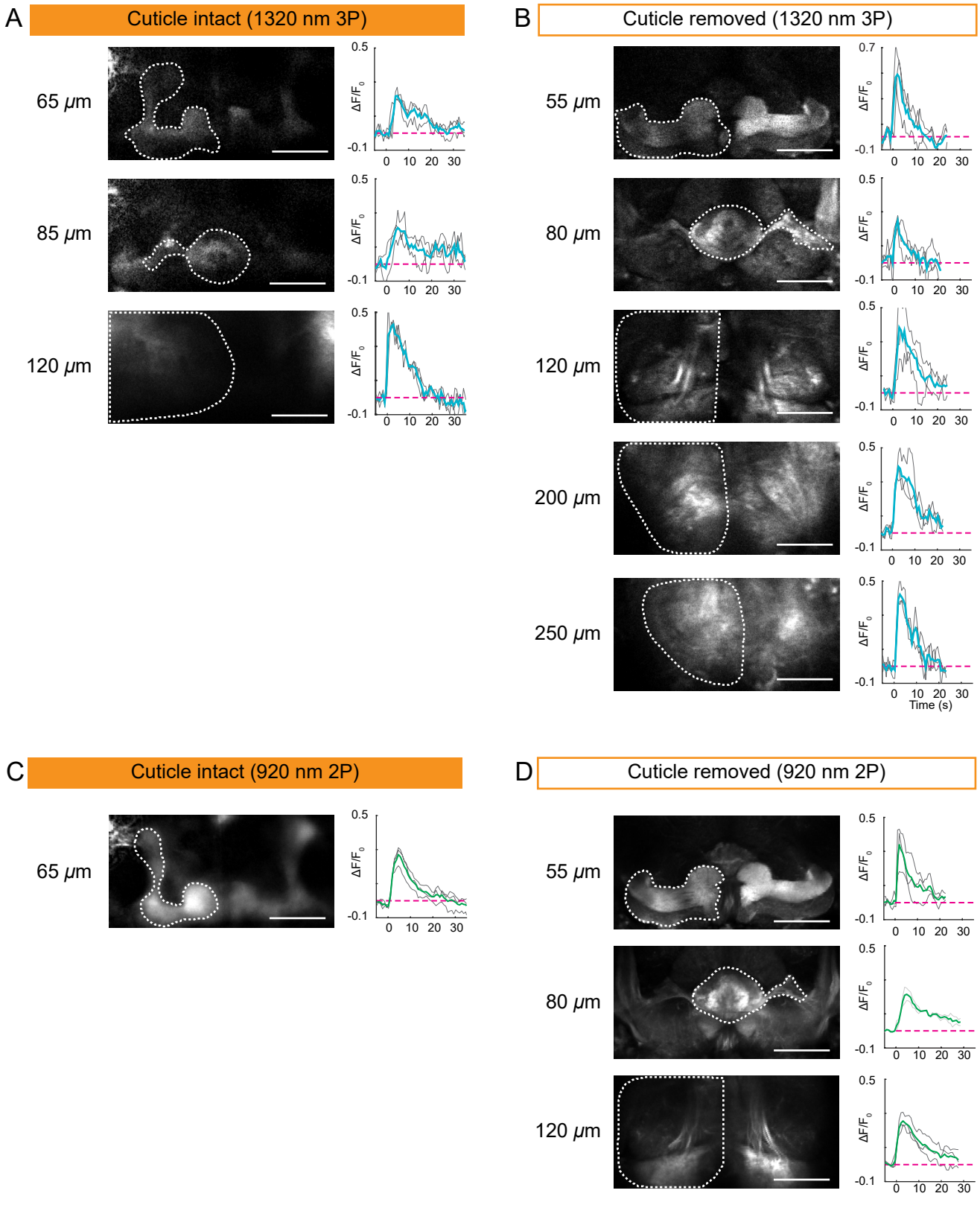
A
Cuticle intact (1320 nm 3P)
65 μm
85 μm
120 μm
B
Cuticle removed (1320 nm 3P)
55 μm
80 μm
120 μm
200 μm
250 μm
C
Cuticle intact (920 nm 2P)
65 μm
D
Cuticle removed (920 nm 2P)
55 μm
80 μm
120 μm
ΔF/F0
Time (s)

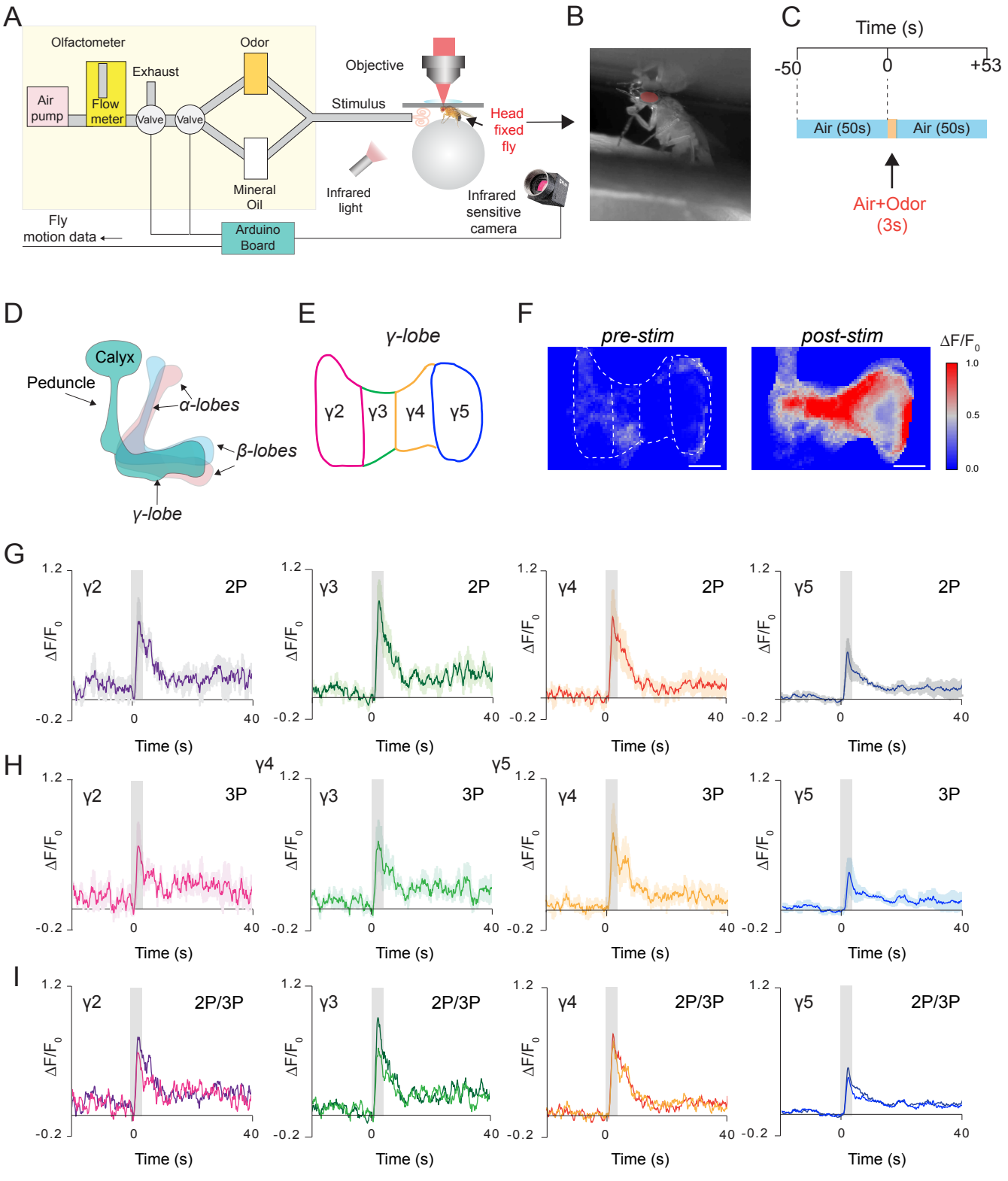
A
Olfactometer
Odor
Exhaust
Air pump
Flow meter
Valve
Valve
Objective
Stimulus
Head fixed fly
Mineral Oil
Infrared light
Infrared sensitive camera
Fly motion data
Arduino Board
B
C
Time (s)
-50
0
+53
Air (50s)
Air (50s)
Air+Odor (3s)
D
Calyx
Peduncle
α-lobes
β-lobes
γ-lobe
E
γ-lobe
γ2
γ3
γ4
γ5
F
pre-stim
post-stim
ΔF/F0
1.0
0.5
0.0
G
γ2 2P
γ3 2P
γ4 2P
γ5 2P
ΔF/F0
1.2
-0.2
0
40
Time (s)
H
γ2 3P
γ3 3P
γ4 3P
γ5 3P
I
γ2 2P/3P
γ3 2P/3P
γ4 2P/3P
γ5 2P/3P

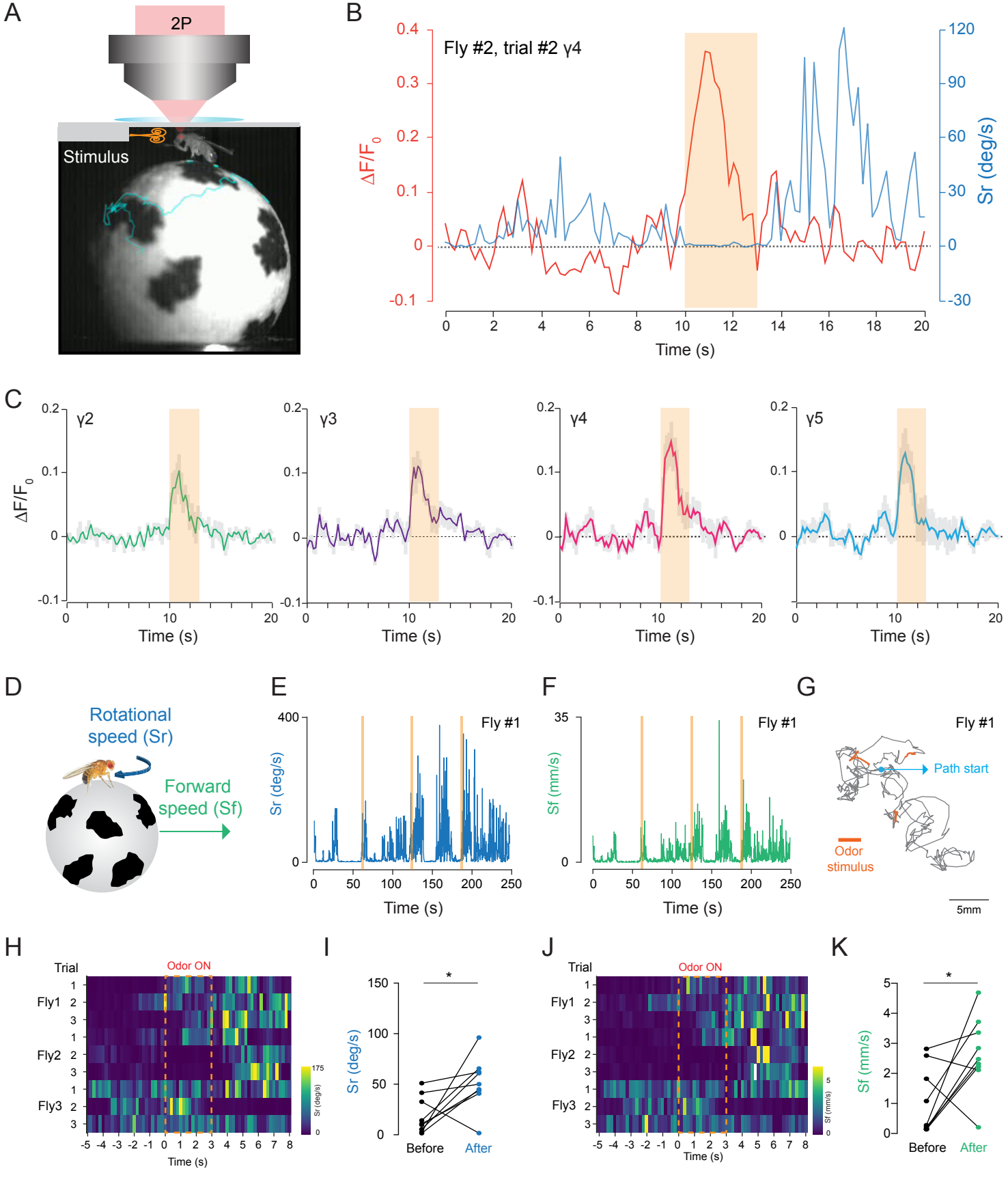
A
2P
Stimulus
B
Fly #2, trial #2 γ4
ΔF/F0
Sr (deg/s)
Time (s)
C
γ2
γ3
γ4
γ5
ΔF/F0
Time (s)
D
Rotational speed (Sr)
Forward speed (Sf)
E
Fly #1
Sr (deg/s)
Time (s)
F
Fly #1
Sf (mm/s)
Time (s)
G
Fly #1
Path start
Odor stimulus
5mm
H
Trial
Odor ON
Fly1
Fly2
Fly3
Time (s)
Sr (deg/s)
I
Sr (deg/s)
Before
After
J
Trial
Odor ON
Fly1
Fly2
Fly3
Time (s)
Sf (mm/s)
K
Sf (mm/s)
Before
After

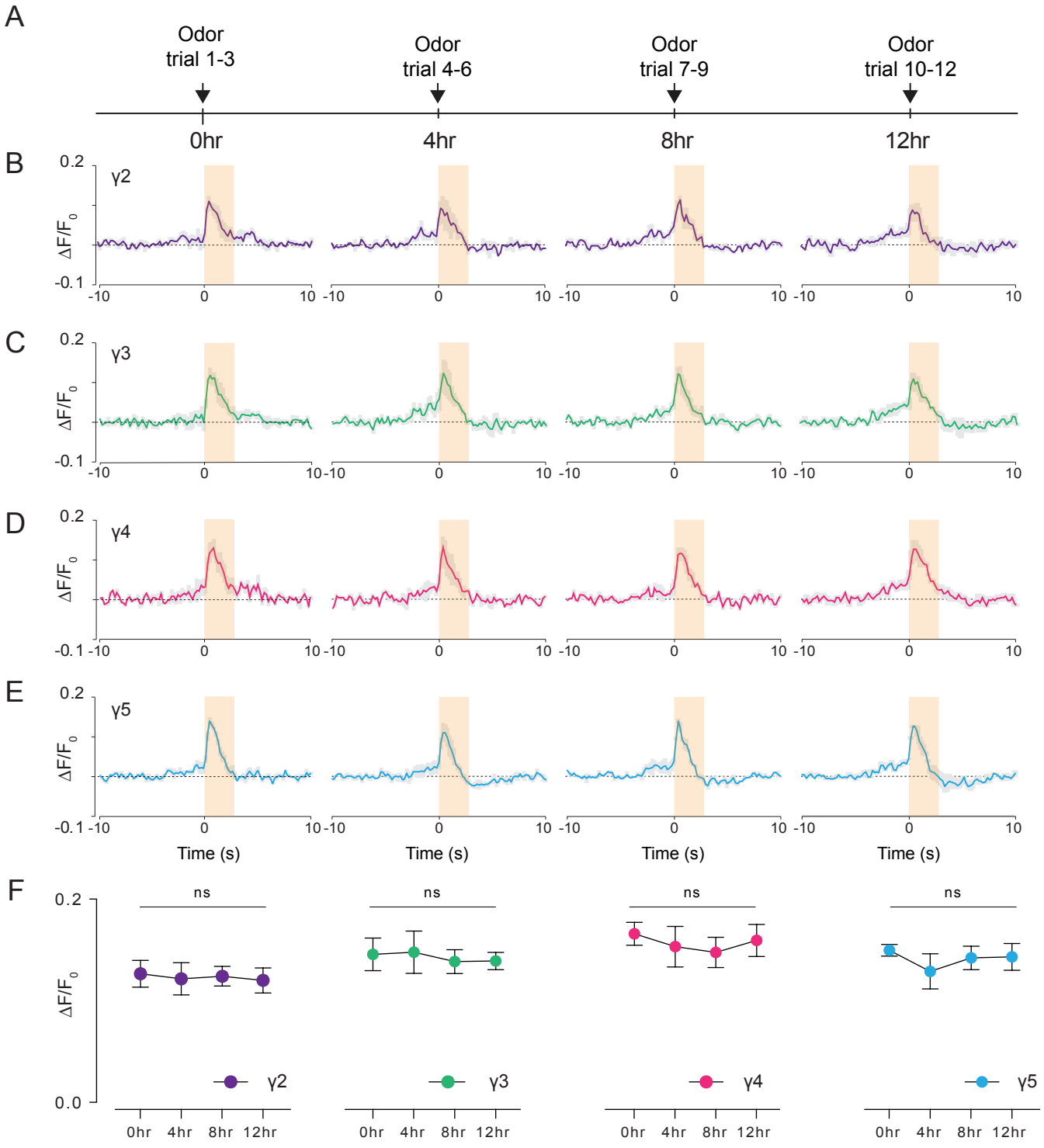
A
Odor trial 1-3
Odor trial 4-6
Odor trial 7-9
Odor trial 10-12
0hr
4hr
8hr
12hr
B
γ2
C
γ3
D
γ4
E
γ5
ΔF/F0
0.2
-0.1
-10
0
10
Time (s)
F
ns
0.0
γ2
γ3
γ4
γ5
0hr 4hr 8hr 12hr

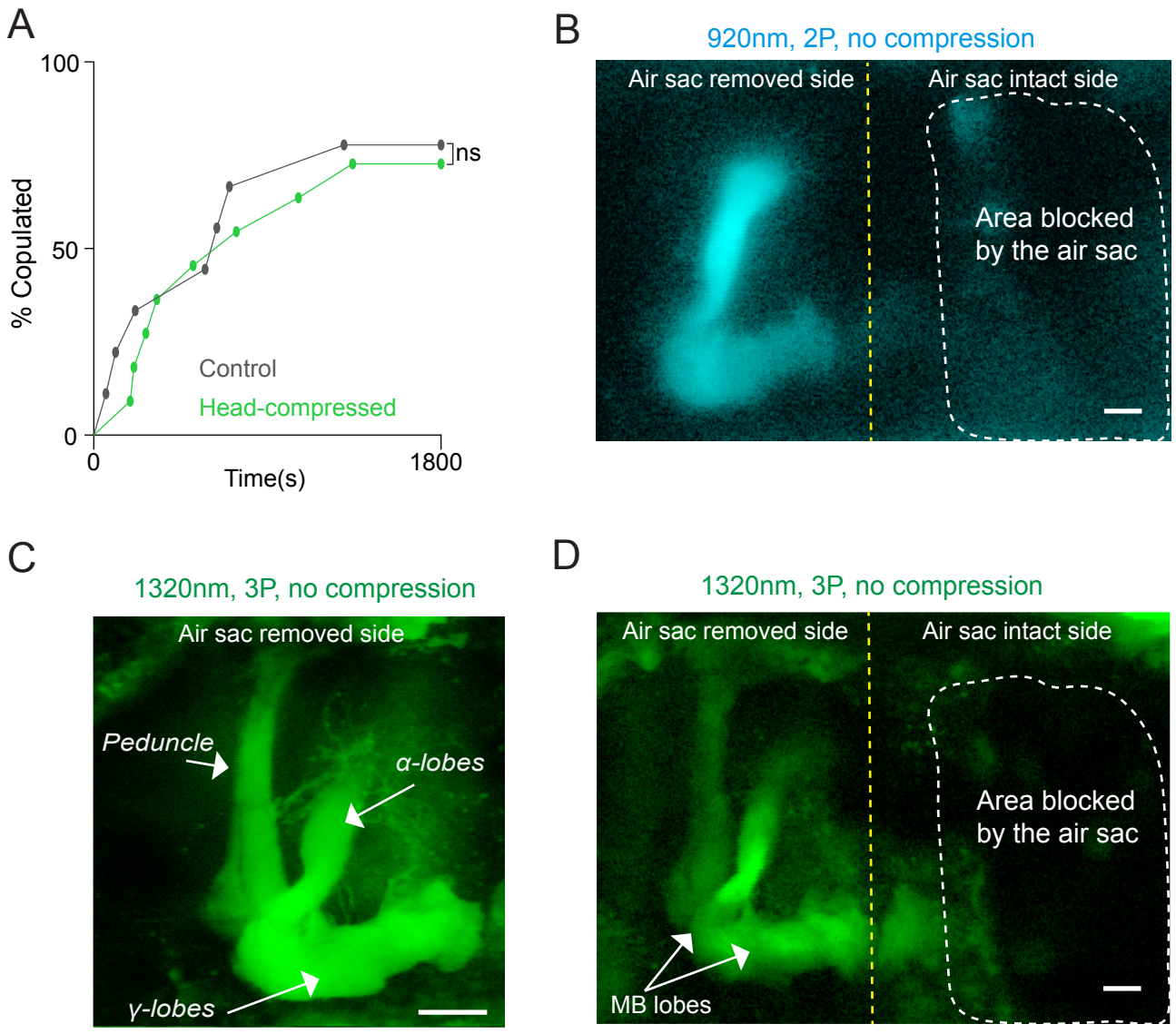
A
100
50
0
% Copulated
0
1800
Time(s)
ns
Control
Head-compressed
B
920nm, 2P, no compression
Air sac removed side
Air sac intact side
Area blocked
by the air sac
C
1320nm, 3P, no compression
Air sac removed side
Peduncle
α-lobes
γ-lobes
D
1320nm, 3P, no compression
Air sac removed side
Air sac intact side
Area blocked
by the air sac
MB lobes

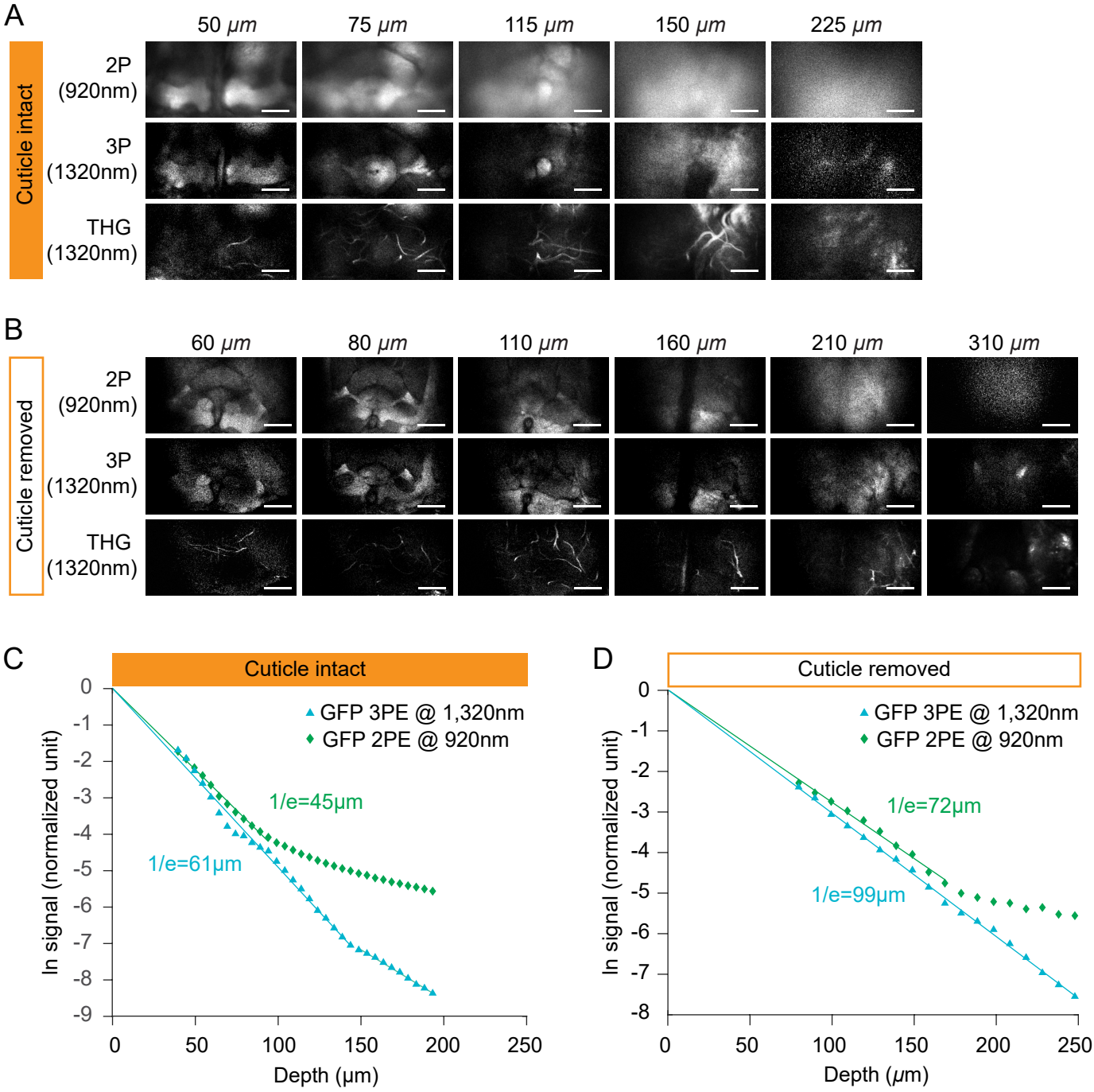
A
50 μm
75 μm
115 μm
150 μm
225 μm
Cuticle intact
2P (920nm)
3P (1320nm)
THG (1320nm)
B
60 μm
80 μm
110 μm
160 μm
210 μm
310 μm
Cuticle removed
2P (920nm)
3P (1320nm)
THG (1320nm)
C
Cuticle intact
GFP 3PE @ 1,320nm
GFP 2PE @ 920nm
1/e=45μm
1/e=61μm
ln signal (normalized unit)
Depth (μm)
D
Cuticle removed
GFP 3PE @ 1,320nm
GFP 2PE @ 920nm
1/e=72μm
1/e=99μm
ln signal (normalized unit)
Depth (μm)

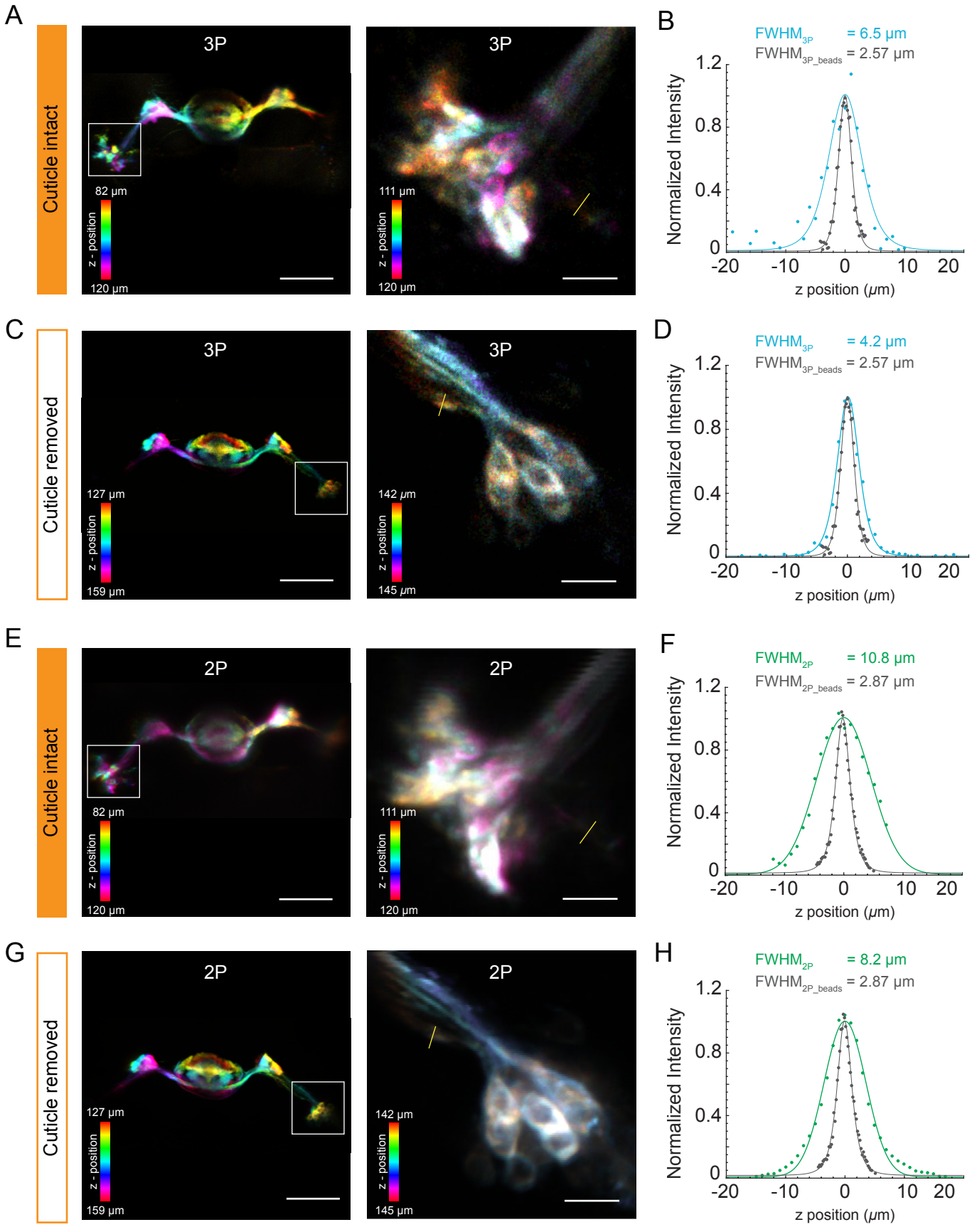
A
Cuticle intact
3P
82 µm
z - position
120 µm
3P
111 µm
z - position
120 µm
B
FWHM3P = 6.5 µm
FWHM3P_beads = 2.57 µm
Normalized Intensity
z position (µm)
C
Cuticle removed
3P
127 µm
z - position
159 µm
3P
142 µm
z - position
145 µm
D
FWHM3P = 4.2 µm
FWHM3P_beads = 2.57 µm
Normalized Intensity
z position (µm)
E
Cuticle intact
2P
82 µm
z - position
120 µm
2P
111 µm
z - position
120 µm
F
FWHM2P = 10.8 µm
FWHM2P_beads = 2.87 µm
Normalized Intensity
z position (µm)
G
Cuticle removed
2P
127 µm
z - position
159 µm
2P
142 µm
z - position
145 µm
H
FWHM2P = 8.2 µm
FWHM2P_beads = 2.87 µm
Normalized Intensity
z position (µm)

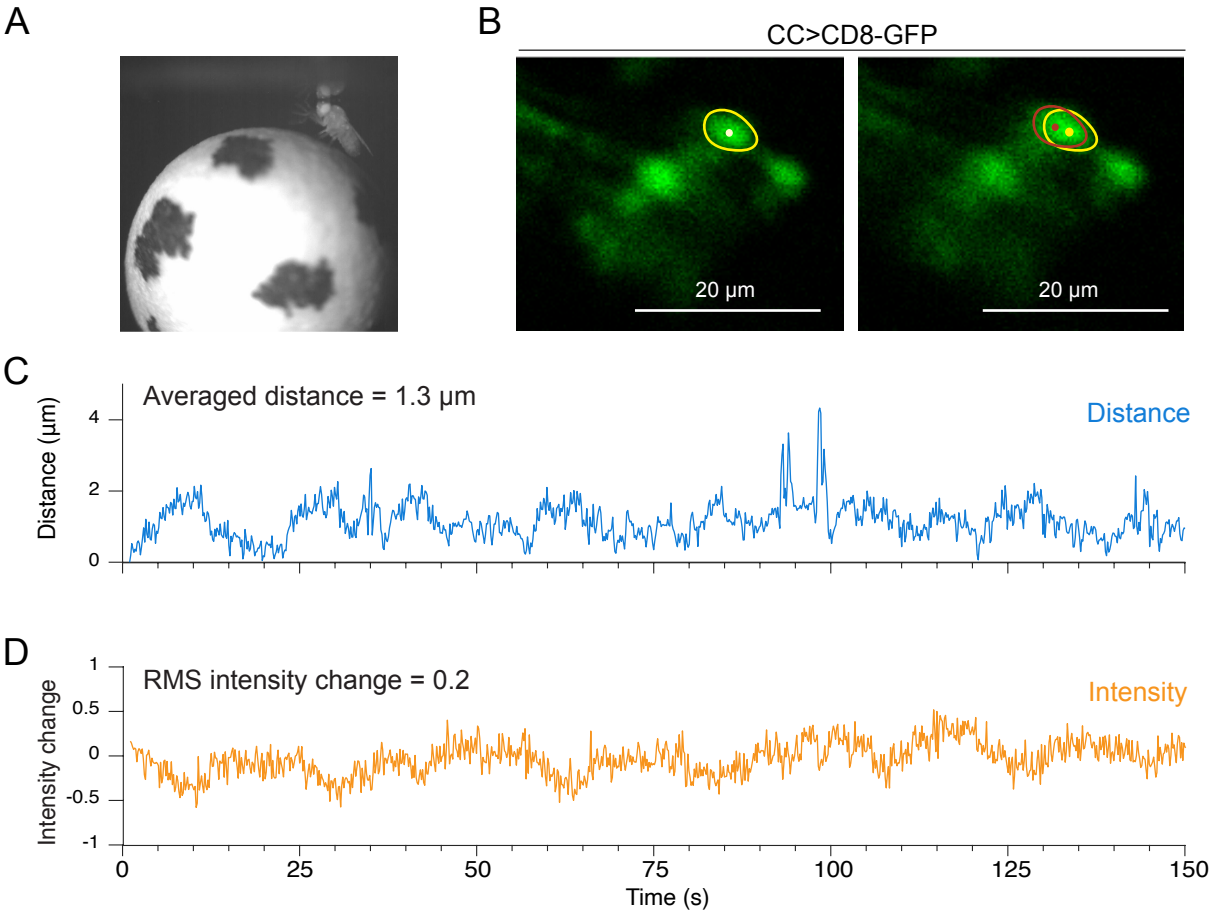
A
B
CC>CD8-GFP
20 µm
20 µm
C
Averaged distance = 1.3 µm
Distance
Distance (µm)
4
2
0
D
RMS intensity change = 0.2
Intensity
Intensity change
1
0.5
0
-0.5
-1
0
25
50
75
100
125
150
Time (s)

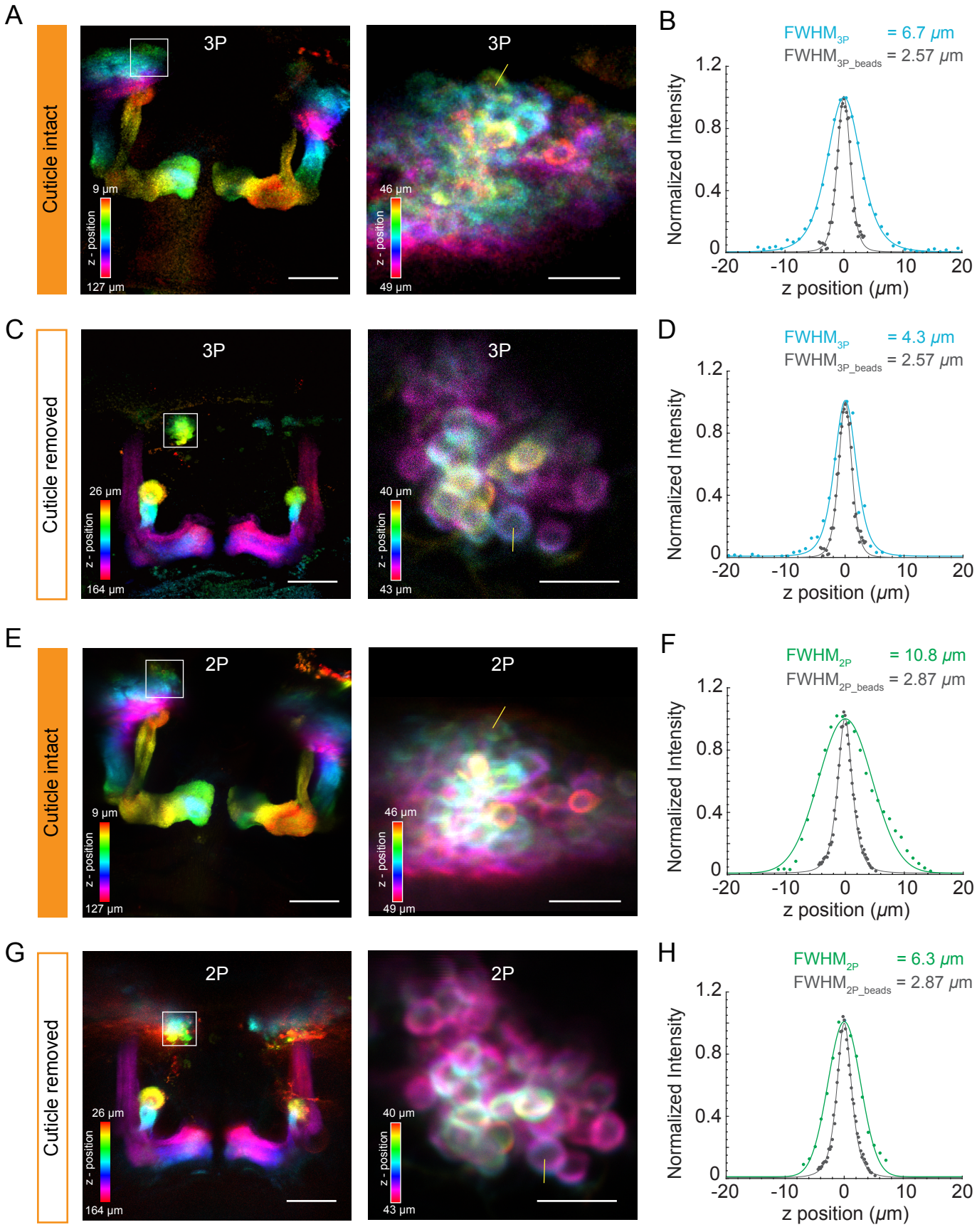
A
Cuticle intact
3P
9 µm
z - position
127 µm
3P
46 µm
z - position
49 µm
B
FWHM3P = 6.7 µm
FWHM3P_beads = 2.57 µm
Normalized Intensity
1.2
0.8
0.4
0
-20
-10
0
10
20
z position (µm)
C
Cuticle removed
3P
26 µm
z - position
164 µm
3P
40 µm
z - position
43 µm
D
FWHM3P = 4.3 µm
FWHM3P_beads = 2.57 µm
Normalized Intensity
1.2
0.8
0.4
0
-20
-10
0
10
20
z position (µm)
E
Cuticle intact
2P
9 µm
z - position
127 µm
2P
46 µm
z - position
49 µm
F
FWHM2P = 10.8 µm
FWHM2P_beads = 2.87 µm
Normalized Intensity
1.2
0.8
0.4
0
-20
-10
0
10
20
z position (µm)
G
Cuticle removed
2P
26 µm
z - position
164 µm
2P
40 µm
z - position
43 µm
H
FWHM2P = 6.3 µm
FWHM2P_beads = 2.87 µm
Normalized Intensity
1.2
0.8
0.4
0
-20
-10
0
10
20
z position (µm)

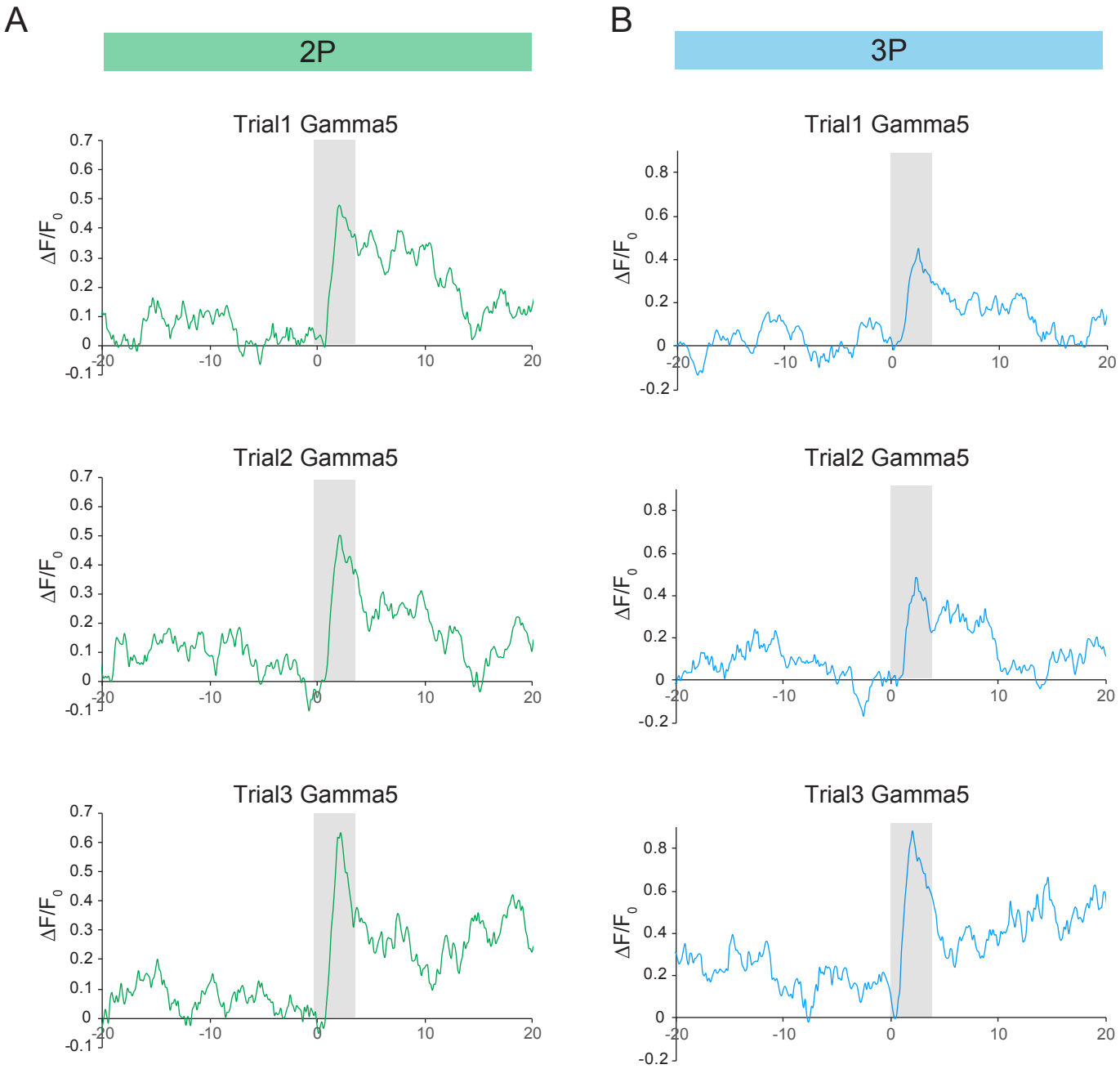
A
2P
B
3P
Trial1 Gamma5
Trial2 Gamma5
Trial3 Gamma5
ΔF/F0

anti-BRP, anti-GFP, anti-HSP70

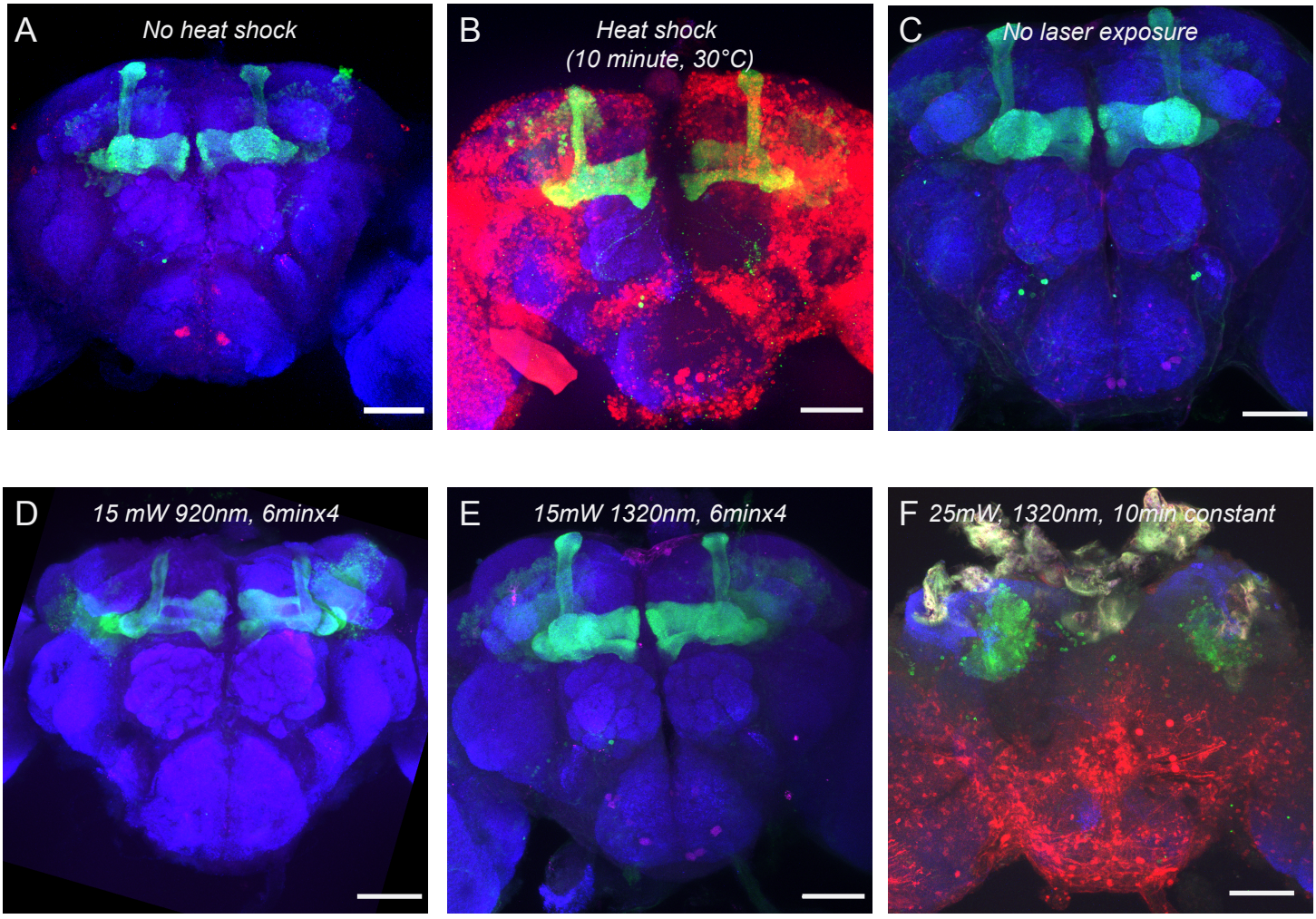

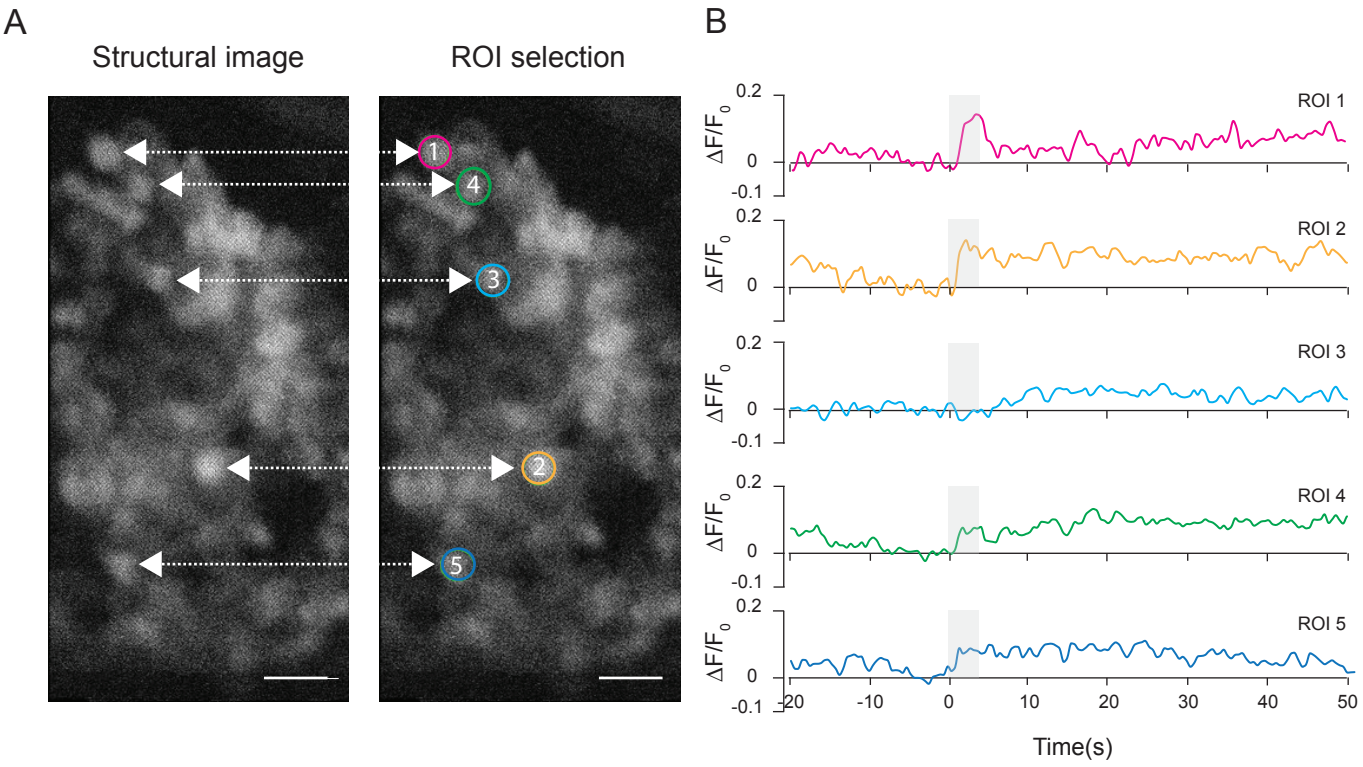
A
Structural image
ROI selection
1
4
3
2
5
B
ROI 1
ROI 2
ROI 3
ROI 4
ROI 5
ΔF/F0
0.2
0
-0.1
-20
-10
0
10
20
30
40
50
Time(s)